metals

MDPI

Review

Corrosion of Cast Aluminum Alloys: A Review

C. Berlanga-Labari [1,*], M.V Biezma-Moraleda [2] and Pedro J. Rivero [1]

[1] Engineering Department, Institute for Advanced Materials and Mathematics (INAMAT[2]), Public University of Navarre, Campus Arrosadía s/n, 31006 Pamplona, Spain; pedrojose.rivero@unavarra.es

[2] Department of Earth, Materials Science and Engineering, University of Cantabria, 39004 Santander, Spain; maria.biezma@unican.es

* Correspondence:carlos.berlanga@unavarra.es

Received: 23 September 2020; Accepted: 13 October 2020; Published: 16 October 2020

Abstract: Research on corrosion resistance of cast aluminum alloys is reviewed in this article. The effect of the main microstructural features of cast aluminum alloys such as secondary dendrite arm spacing (SDAS), eutectic silicon morphology, grain size, macrosegregation, microsegregation, and intermetallic compounds is discussed. Moreover, the corrosion resistance of cast aluminum alloys obtained by modern manufacturing processes such as semi-solid and additive manufacturing are analyzed. Finally, the protective effects provided by different coatings on the aluminum cast alloys—such as anodized, plasma electrolytic oxidation (PEO), and laser—is reviewed. Some conclusions and future guidelines for future works are proposed.

Keywords: corrosion, aluminum alloys, semisolid manufacturing (SSM), additive manufacturing (AM), coatings

1. Introduction

The use of cast aluminum alloys has been growing in recent years mainly because of their low density, good castability, high specific strength, and so on. Compared with wrought aluminum alloys, aluminum casting alloys have clear economic advantages such as mass production of components due to their shorter processing cycle and assembly costs. Consequently, the production of aluminum casting components accounts for approximately 60% of annual aluminum production. However, in order to improve casting characteristics and obtain parts with the lowest possible defect content, foundries need a higher content of alloying elements—mainly silicon—which causes a greater tendency to localized corrosion and also prevents the application of the standard anodization treatment; in this way, the corrosion resistance of aluminum castings is considered to be lower than that obtained by forging. As a result, a better understanding of the corrosion resistance and protection of aluminum castings is necessary to overcome this drawback.

In this regard, the purpose of this article is to carry out an orderly and complete review of the corrosion of cast aluminum alloys. The work begins with the revision of corrosion studies performed with alloys obtained by traditional casting processes such as sand, metal die cast, and high pressure die casting (HPDC) (Sections 1 and 2).

In Section 3, the research on aluminum cast alloys obtained by semi-solid processes (SSM) is discussed while Section 4 is dedicated to reviewing the recent works about cast aluminum alloys obtained by additive manufacturing (AM). Section 5 focuses on the corrosion resistance of the different coatings applied to aluminum castings.

The relationship of the procedures for manufacturing aluminum castings alloys with the microstructure and the resistance to corrosion has been highlighted. In summary, this review article presents a comprehensive review of the most recently published studies dealing with the corrosion of cast aluminum alloys.

2. Corrosion Resistance of Cast Aluminum Alloys

Some researchers use standardized aluminum alloys for their research while others manufacture their own alloys. In this review, the designation systems for aluminum castings proposed by the Aluminum Association (AA) has been adopted (Table S1).

2.1. Series 3xx.x

The 300 series alloys are alloyed with silicon and magnesium and/or Cu. Due to their good mechanical properties and appropriate casting characteristics, 90% of the aluminum castings produced worldwide belong to the 300 series. Most of the cast aluminum alloys in this series are devoted to the automotive market for applications such as chassis, engine components, etc.

Thus, alloys belonging to the 300 series have been the most used to perform corrosion studies with cast aluminum alloys.

2.1.1. Corrosion Resistance of Cast Aluminum Alloys Obtained by Gravity Castings

Aluminum castings can be classified according to the nature of the mold used (sand or metal) or depending on the way the aluminum is melted (gravity, low pressure, and high pressure). The corrosion studies of the 300 series alloys obtained by gravity in metal and sand mold are reviewed in this section.

The microstructure and macrostructure of aluminum cast aluminum alloys depend on different factors such as alloys used, cooling rates during solidification, and micro and macrosegregation. Osorio et al. have done several works analyzing in detail these factors in the corrosion resistance of aluminum cast alloys [1,2].

In this regard, Osorio et al. [1] evaluated the local effects of Si and Cu contents and secondary dendrite arm spacing (SDAS) on the corrosion behavior of directionally solidified ternary Al-Cu-Si alloys castings (Al-6Cu-1Si and Al-8Cu-3Si). Samples near the mold–metal interface (10 mm) and far from the interface (60 mm) were taken in order to estimate the influence of cooling rate.

From the results observed (Table S2), they concluded that corrosion current density and impedance parameters of the Al-8Cu-3Si are more corrosion resistant than Al-6Cu-1Si independently of the scale of the dendrite array. Moreover, the Si content had not affected the corrosion performance along the inverse Cu profile analyzed.

In another work, Osorio et al. [2] evaluated the corrosion resistance of Al-6%Cu-1%Si alloy casting taking into consideration the combined effect of Si, macrosegregation profiles, and secondary dendrite arm spacing (SDAS).

In the Figure 1, locations in the casting from where the samples for corrosion test were extracted are indicated. It is worth noting that the corrosion test was carried out in transverse sections of the castings at 0, 10, and 20 mm from the casting cooled surface.

These results obtained (Table S2) and not in agreement with those of binary Al-Si and Al-Cu alloys, with had indicated higher corrosion resistance for coarse and fine dendritic microstructures, respectively. These findings indicate that Si Content and SDAS can play an interdependent role in the corrosion behavior of an Al-Cu-Si alloy. On the one hand, the phenomenon of inverse segregation of Cu causes a decrease in corrosion resistance, but on the other hand the refinement of the dendritic array below 15 μm, decreases the corrosion rate.

Due to the low solubility of most solutes in the α aluminum matrix, cast aluminum alloys are prone to the formation of intermetallic compounds. Culliton et al. [3] reviewed the most common intermetallic phases found in the aluminum alloys taking into account their size, morphology, and corrosion potential. However, few studies have been carried out to examine in detail the influence of the corrosion resistance of intermetallic compounds on cast aluminum alloys.

Dobkowska et al. [4] reported the influence of the formation of intermetallic compounds of AlFeSi, AlMnFeSi, and AlMgFeSi on the corrosion resistance of AlSi5, AlSi7Mg, and AlSi10Mg. The measured corrosion densities were significantly lower than those obtained by other authors using similar alloys (Table S2). This can be explained by the low concentration of NaCl used in the tests (0.1

M) compared to most other works (0.5 M); although they found similar corrosion potentials, they concluded that AlSiMg10 alloy exhibited less damage because the presence of Mn compensated for the cathodic effect of Fe in intermetallic compounds. In Figure 2, it is presented the formation of intermetallic compounds $Al_9FeMg_3Si_5$, β-AlFeSi, and α-AlFeMn Si in AlSi7Mg alloy (Figure 2a), whereas only α-AlFeMn Si compound is identified in Figure 2b.

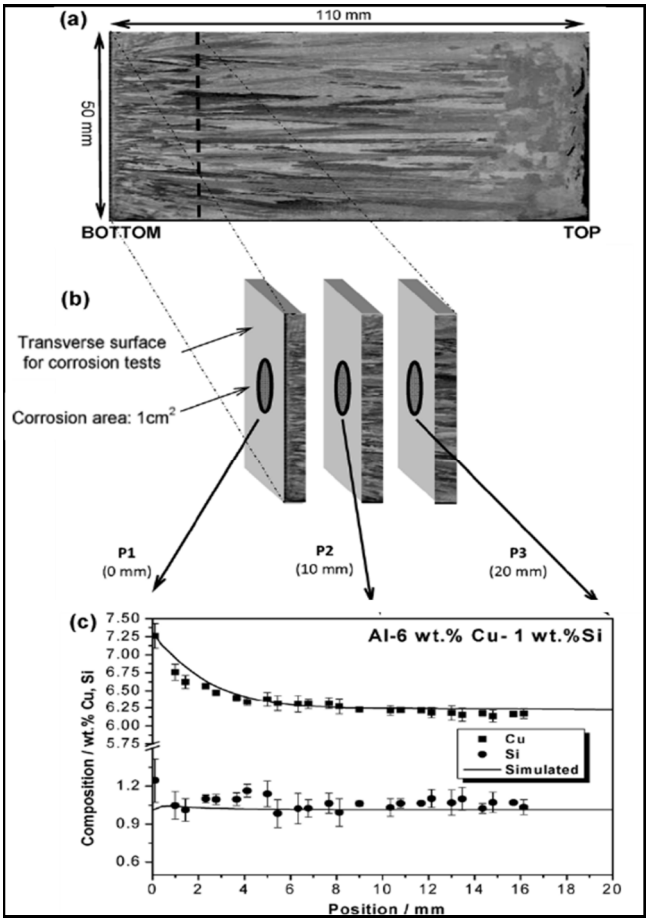

Figure 1. (**a**) Typical macrostructure of an Al–6 wt %, Cu–1 wt % Si alloy, (**b**) representation of the transverse surface samples used in the corrosion tests, and (**c**) experimental and simulated Cu and Si profiles corresponding to positions close to the casting surface highlighting the Cu macrosegregation. Reprinted with permission of [2].

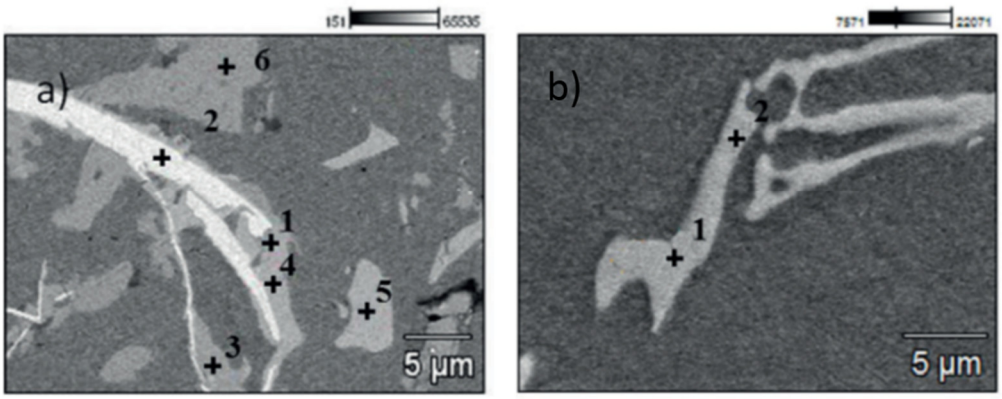

Figure 2. SEM micrographs and EDS analysis performed in (**a**) $AlSi_7Mg$ and (**b**) $AlSi_{10}Mg$, respectively. Reprinted with permission of [4].

Eutectic modification is usually performed to change the morphology of eutectic Si from a circular morphology to a fibrous structure in the range of 50–200 ppm. Although numerous studies have been carried out to determine the effect of the modifying elements such as Na, Sr, or even Sb on the mechanical properties, few studies have been focused on their effect on the corrosion resistance.

The effect of adding Sr to an A-356 alloy was studied by Ozturk [5]. They carried out the modification by adding different percentages of Sr 120, 170, and 250 ppm to an A-356 alloy obtained by die cast and sand cast mold. At microstructural level, they observed a modification of the eutectic silicon from a coarse acicular morphology to a fibrous morphology, as it is appreciated in Figure 3. This effect was more evident in sand cast samples than in die cast because the lower cooling rate promotes the growth of silicon.

The addition of Sr led to a significant reduction in the corrosion rate from 13.8 μA/cm^2 to 0.42 μA/cm^2 for 120 ppm Sr addition in die cast while going from 10.2 μA/cm^2 to 1.47 μA/cm^2 for when 150 ppm was added in sand mold. As a result, it can be seen that the modification of eutectic silicon significantly improves the general corrosion resistance as it allows the formation of a more stable passive layer. However, the addition of Sr did not improve pitting corrosion resistance as no passive plateau was observed in any sample.

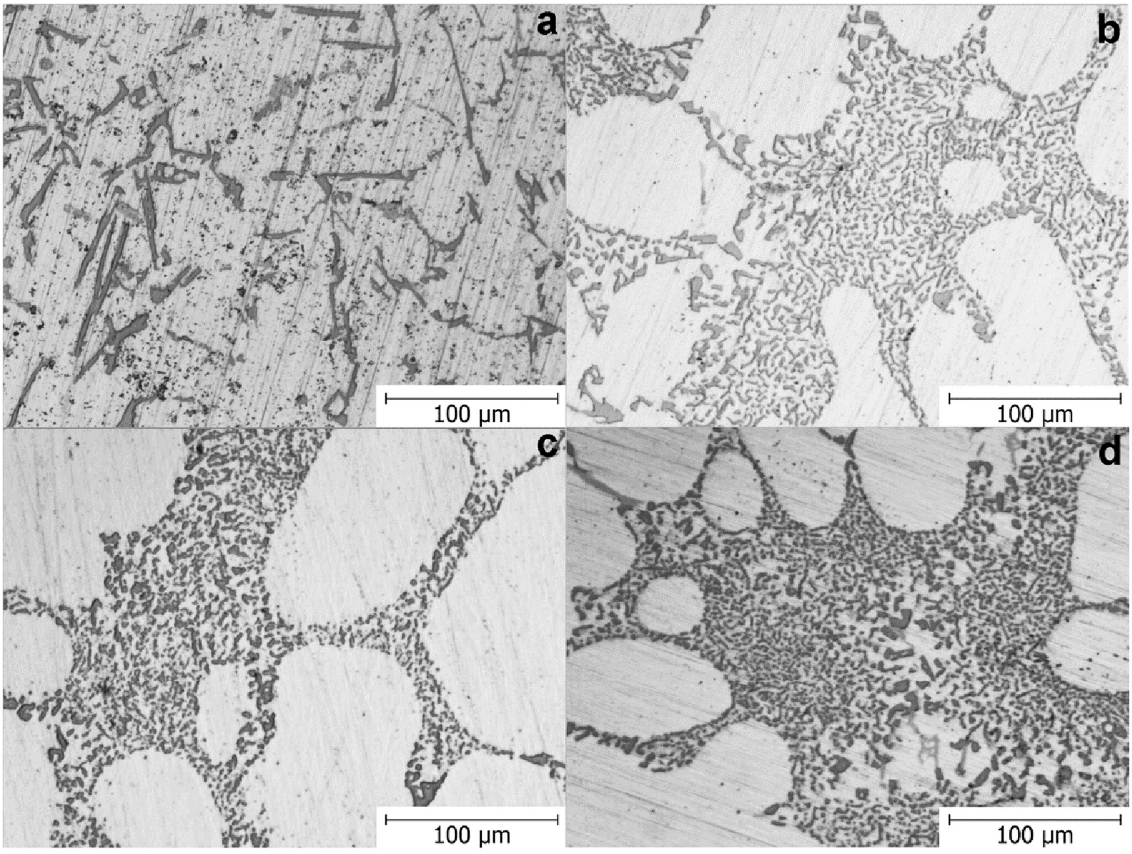

Figure 3. Microstructure images of A356 cast samples with different Sr addition (**a**) No Sr addition, (**b**) 120 ppm, (**c**) 170 ppm, and (**d**) 250 ppm. Reprinted with permission of [5].

Although most of the corrosion experimentation is carried out in chloride-rich media, it is also necessary to test corrosion behavior in other media where aluminum cast alloys are also used.

Zor et al. [6] investigated the effect of the Cu content between 1% and 5% of an Al-Si alloy in solutions 0.1M HCl and 0.1 M H_2SO_4. They cast the alloys in a permanent steel mold and then carried out an ageing heat treatment (no details were provided about the heat treatment). In order to evaluate corrosion resistance in acidic media, they carried out electrochemical impedance spectroscopy (EIS) tests and measured the evolution of H_2(g) formation in immersion tests. The results showed a

contradictory effect of Cu since on the one hand it caused a decrease in the corrosion rate of both HCl and H_2SO_4 (Table S2) while on the contrary, Cu promoted the formation of intergranular corrosion.

Sekularak et al. [7] studied the corrosion resistance of an A-356 as-cast alloy in synthetic seawater with different Na_2S contents of 20, 50, and 100 ppm in a 42-day immersion test.

Figure 4 shows how the composition and structure of the oxide formed depends on the Na_2S concentration and the test time. At low Na_2S (20 ppm) they measured a low current density of 4.5x 10^{-9} A cm^2 and a high passivation range of 0.94V after 14 days of immersion test. This behavior was associated with the formation of a compact and crystalline aluminum hydroxide layer. The addition of 50 and 100 ppm of Na_2S caused the deposition of Mg ions and the formation of an extra outer layer of spinel and MgO, which provided additional corrosion resistance for the first 21 days only.

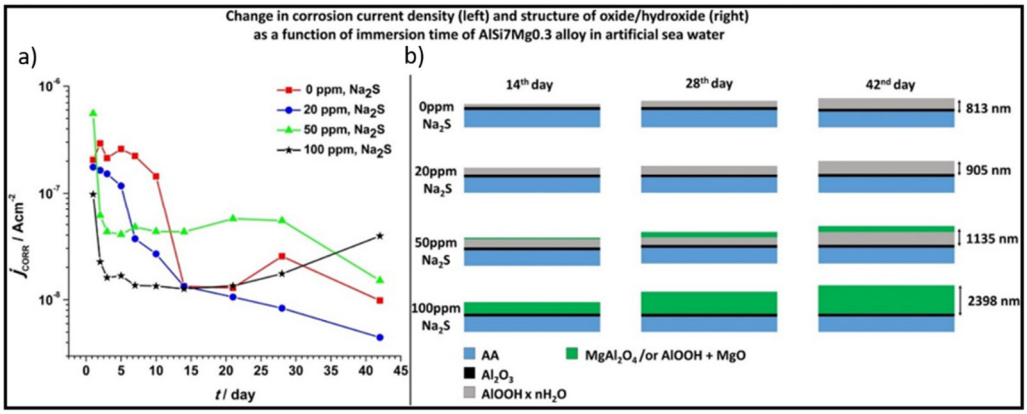

Figure 4. (**a**) Change in corrosion density as a function of immersion time. (**b**) Schematic presentation of oxide layer formation at the surface of AA EN-AlSi7Mg0.3 during the course of immersion in artificial sea water with added Na_2S. Reprinted with permission of [7].

Although the T6 heat treatment is the most used to improve the mechanical properties of the 300 series alloys, others can also be made. In this regard, Panagopoulos et al. [8] evaluated the corrosion resistance in a A319 alloy with different thermal treatments: T1, T5, and T6; in addition to the T6 treatment, they also performed a variant of the T6 thermal treatment which consisted of carrying out two steps in the solution treatment.

The results showed that the best performance corresponded to the T6 heat treatment performed in two steps (95 μAcm²) while the treatment T6 performed in one step showed a slightly higher corrosion rate of 105 μAcm². Finally, the T1 (190 μAcm²) and T5 (260 μAcm²) heat treatments showed the worst behavior. On the other hand, it should be noted that unlike most studies where neutral chlorides have been used, a basic pH has been used in this work (pH–12), which has led to significantly higher corrosion rates. This observation is justified on the basis of Pourbaix's diagrams, which shows that at basic pHs, no protective Al_2O_3 is formed as at neutral pHs link to an active dilution of the aluminum.

2.1.2. Influence of Addition of Rare Earths on Corrosion Resistance

One of the strategies followed to improve the microstructure and mechanical properties of aluminum cast alloys has been the addition of rare earths (RE). However, very few articles have been written investigating the effect of the addition of rare earths on the corrosion resistance of cast aluminum alloys.

Arrabal et al. [9] investigated the effect of the addition of 0.38% Nd on the microstructure and corrosion behavior of an A356 alloy obtained by gravity and compared it to an A356 alloy without Nd. By means of the SKPFM technique they obtained maps of superficial potentials to determine the anodic or cathodic nature of the intermetallic compounds and microstructural elements with respect to the matrix. In addition, polarization tests also revealed improved behavior of the alloy at 356 Nd with a passive region of 180 mV while the Nd-free alloy showed stable pitting growth.

It was concluded that the addition of Nd improved the pitting resistance due to a refinement of the microstructure and elimination of microgalvanic pairs between the intermetallic compounds and the aluminum matrix. They associated this finding with the formation of intermetallic compounds (Figure 5) that are less harmful from a corrosion point of view since they measured a lower potential difference with respect to the α Al matrix than the intermetallic compounds observed in aluminum cast such as β-Al_5FeSi.

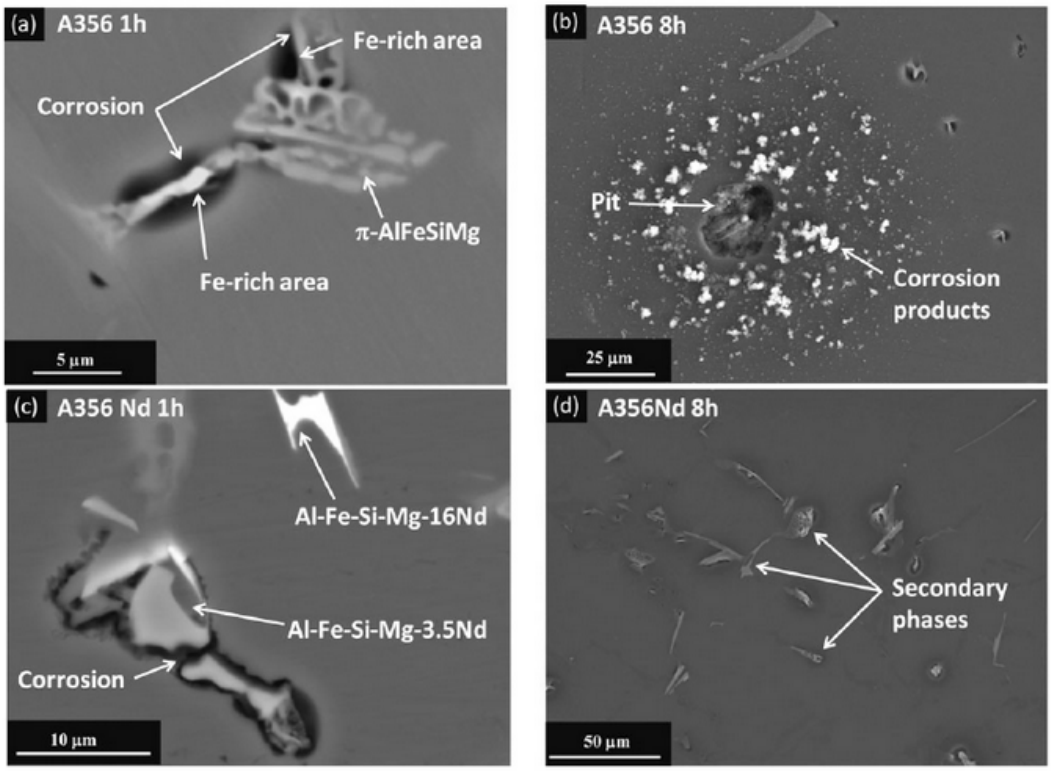

Figure 5. SEM micrographs of the initial stages of corrosion attack of A356 (**a**,**b**) and A356Nd (**c**,**d**) alloys as a function of time: (**a**,**c**) 1 h, (**b**,**d**) 8 h. Reprinted with permission of [9].

Liang et al. [10] investigated a new aluminum alloy (Si = 11.7%, Fe = 0.18%, Sr = 0.14%) with a low Cu content and an addition of 1.44% rare earths (La, Ce, and Nd) and compared it with the A 360 (Cu = 0.56%) and A380 (Cu = 3.57%) alloys. A permanent steel mold preheated to 250 °C, and then aged at 180 °C for 4 h, was used. These rare earths have produced a dramatic microstructure refinement and eutectic silicon morphology modification with much better homogeneous distribution of the second particles in the matrix.

The new alloy showed a corrosion rate of 0.083 mm/year while the A360 alloy 0.104 m/year and the A380 m/year alloy 0.150 after a 240 h NaCl 3.5% immersion test. Polarization tests also indicated improved corrosion behavior in the new alloy (1.04 $\mu A/cm^2$) as compared to the A360 alloy (1.42 $\mu A/cm^2$) and the A380 alloy (1.56 $\mu A/cm^2$) They concluded that the higher corrosion resistance of the new alloy was related to the modification of the morphology of the Si present in the eutectic and to the improvement of the homogeneity of the dispersion of the intermetallic compounds.

Zou et al. [11] studied the effect of adding Yb in a concentration range between 0 and 1.2% to an ADC12 alloy obtained by gravity in a metal mold. They found an optimal corrosion resistance in the alloy containing 0.9% Yb with a minimum weight loss rate of 46 $\mu g cm^{-2} day^{-1}$ (Figure 6) after a 30 days of corrosion immersion test.

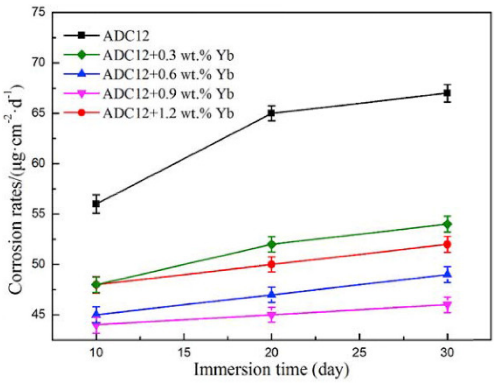

Figure 6. Weight loss rate curves of ADC12-xYb aluminum alloys immersed in 3.5 wt % NaCl solution for 10, 20, 30 days. Reprinted with permission from Elsevier [11].

Moreover, they measured a corrosion current density of 1.27 μA/cm² for this alloy which is 84.7% lower than the unmodified alloy (8.30 μAcm²). The improved corrosion resistance was due to the formation of Al_3Yb intermetallic precipitates as they form a protective layer on the Si surface suppressing the corrosive activity of the cathodic region.

The corrosion resistance of an AlSi5Cu1Mg alloy with different La additions (0.3%, 0.6%, and 0.9%) was examined [12]. It was highlighted that the optimal La addition was 0.6 % reducing the corrosion rate by 40% (from 54 to 22 μAcm²) with respect to the La-free alloy as showed in Table S3.

They suggested that this improvement in corrosion resistance was due to the formation of a La rich coating over the cathodic phases, thus the decrease in the electronic current between the anode and the cathode. It was also noted that when La content increases to 0.9%, the formation of La-Al-Cu intermetallics compounds leads to microgalvanic corrosion with the Al matrix and increasing the corrosion rate.

The effect of the corrosion resistance of Er and Zr on an A-356 alloy obtained by permanent metal mold was studied by Colombo et al. [13]. By performing immersion corrosion tests, they observed that the addition of Er decreased the corrosion rate from 45.8 μg/cm²d to 4.2 μg/cm²d and they associated this improvement with the modification of the morphology of eutectic silicon from laminar to globular. They also noted that the zirconium-containing alloy had a greater corrosive attack due to the greater presence of intermetallic compounds.

2.1.3. Corrosion Resistance of Cast Aluminum Alloys Obtained by High Pressure Die Casting (HPDC)

HPDC technology is frequently used to produce cast aluminum components for the transportation industry as it has significant advantages such as obtaining complex parts with thin walls and high productivity. Its main disadvantage is the formation of gas bubbles due to the high filling rates of the mold that finally cause a high porosity in the final parts. A possible strategy followed to improve the corrosion resistance of aluminum castings obtained by HPDC has been the optimization of the alloying elements.

Hu et al. [14] compared the corrosion resistance of an alloy obtained by high pressure and permanent mold (HPDC). They measured a better resistance to pitting corrosion in HPDC (Ep = −690 mV) than in permanent mold (Ep = −760 mV) and detected better resistance to intergranular corrosion in the high-pressure alloy which they associated with a finer grain size.

Dos Santos et al. [15] related the parameters of the HPDC process with the microstructure, mechanical properties and corrosion resistance of an AC 46000 alloy. They used three different injection temperatures: 579 °C, 643 °C, and 709 °C and two different injection pressures of 35 MPa and 70 MPa. The microstructure obtained depends on the injection temperature as they observed that at low temperatures the dendrites of α aluminum are fragmented during the HPDC process while at high temperatures the microstructure is more refined. In Figure 7, it is shown the high porosity of all the samples ranged from 3.15% with an injection temperature of 579 °C and 70 MPa to 4.92% with an

injection temperature of 709 °C and 70 MPa. They concluded that the main microstructural factor affecting corrosion resistance is porosity, since the higher the porosity, the lower the corrosion resistance. On the contrary, they found no evident dependence of the formation and distribution of intermetallics with corrosion resistance.

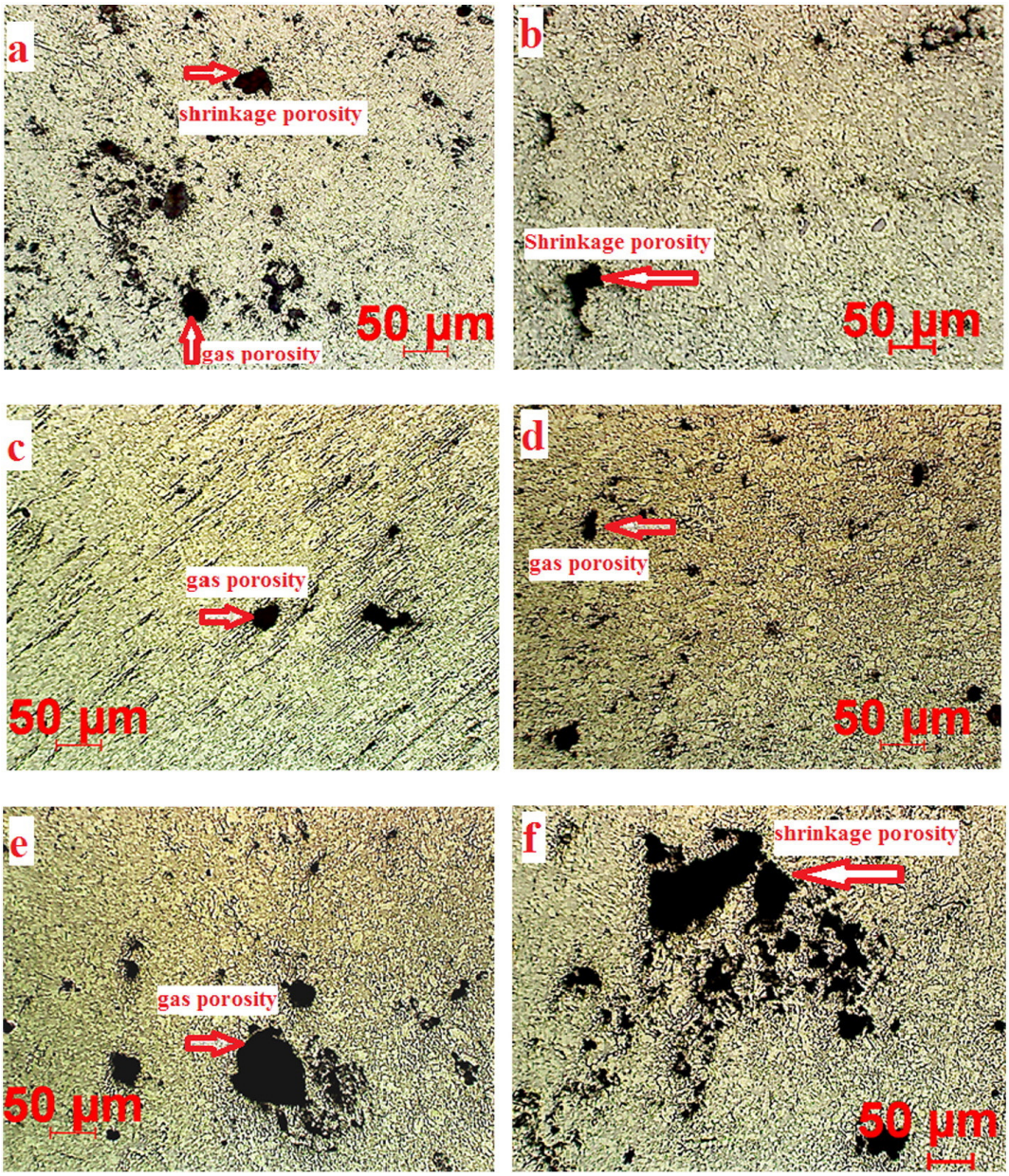

Figure 7. Micrographs of the AlSiCu alloy injected at different combinations of temperature and pressure (**a**) 579 °C/35 MPa, (**b**) 579 °C/70 MPa, (**c**) 643 °C/35 MPa, (**d**) 643 °C/70 MPa, (**e**) 709 °C/35 MPa, and (**f**) 709 °C/70 MPa, respectively. Reprinted with permission of [15].

Most cast aluminum alloys used in automotive components obtained by HPDC belong to the AlSi9CuX family and are obtained from scrap. Although these alloys have a high mechanical strength and hardness, which makes them useful for engine components, they do not have sufficient ductility for structural parts aimed at functions related to structural elements of the vehicle. The major cause of this is the presence of high Fe levels that leads to the formation of β precipitates. In order to avoid these problems, primary aluminum alloys with a lower Fe and Cu content of less than 0.5% and a high percentage of manganese between 0.5% and 0.8% are being used, which is necessary to reduce the die soldering, as well as a Cu content of less than 0.2% to improve corrosion resistance.

Cecchel et al. [16] compared the A380 alloy with 2 structural alloys with low Fe and Cu content: the A360 alloys and the A359. They concluded that the alloys with low Cu and Fe content had a higher passivation range (0.28 V) than the A380 alloy (0.14 V) and they justified this finding by noting the greater presence of aluminum–Cu intermetallic compounds in this alloy.

2.2. Series Other than 3xx.x

2.2.1. Series 1xx.x

The alloys belonging to the 100 series do not contain any alloying elements and are therefore not heat treatable. Since no alloying elements are present in their composition, the main interest has been limited to studying the effect of macro and microstructure on corrosion resistance.

In this regard, Osorio et al. [17] obtained 99.93% pure aluminum by means of a vertical solidification system to obtain a columnar structure. They examined the effect of the macrostructure (equiaxial and columnar) and microstructure (fine grain size and coarse grain size) on corrosion resistance in NaCl 3%. The measured corrosion rates were low (between 0.8 μA/cm^2 up to 2.3 cm^2) compared to other cast aluminum alloys with alloyed elements (Table S4).

2.2.2. Series 2xx.x

The 200 series alloys contain a high Cu content (4–10%) which gives them high mechanical properties. However, the addition of Cu results in a high tendency to the formation of casting defects and consequently the use in industry is limited to the manufacture of components with simple geometries. The effects of Cu content, its tendency to segregation, SDAS, and grain size values as well as macro structure effect have been reviewed by the Osorio group in different works.

If castings are obtained by directional solidification, the macro structure consists of the areas of chill, and columnar and equiaxed regions. Osorio et al. [18] evaluated the effect of grain orientation and SDAS values on the transition zone from the columnar zone to the equiaxial zone (CET) (Figure 8). Although they did not detect large differences in corrosion resistance, they concluded that dendrite arm spacing (SDAS) values have more influence than macro structure.

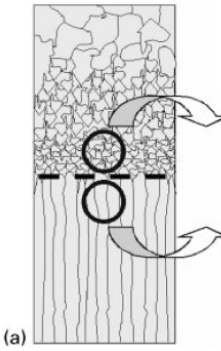

		Columnar (λ_2)	Equiaxed (λ_2)
Al-Cu	Al-5 wt% Cu	61 μm	57 μm
	Al-8 wt% Cu	40 μm	43 μm

(b)

Figure 8. (**a**) Macrostructure representation at CET and (**b**) average values of secondary dendrite arm spacing for Al–5 wt-%Cu and Al–8 wt-%Cu alloys. Reprinted with permission of [18].

Osorio and al. [19] studied the effect of solute redistribution in the matrix and dendritic spacing of an Al-4.5% Cu alloy obtained by directional solidification. Samples were taken in three different positions from the metal-cooler surface (P1, P2, and P3) to determine the effect of the cooling rate and the Cu content. The negative macrosegregation obtained throughout the casting did not have a significant effect on the corrosion resistance of the alloy, as similar corrosion potential and corrosion rates were obtained. At the microscopic level, they observed that the corrosion is located in the eutectic phase within the interdentritic regions. They concluded that the general corrosion rates were better with higher cooling rates, as these resulted in finer dendritic spaces and thus better distribution of the eutectic constituent.

In another work, Osorio et al. [20] verified the effect of different Cu contents (5%, 10%, and 15%) on the corrosion resistance of hypoeutectic Al-Cu alloys. They performed electrochemical tests on 0.5 M H_2SO_4 and measured low corrosion rates (0.45 μA/cm^2) compared to measurements in NaCl 3% media. They concluded that the corrosion rates of the three alloys were similar while the corrosion potential was nobler for the Al-15% Cu alloy.

The alloys included in the 200 series can be heat treated due to their high Cu content. Pournazari et al. [21] carried out a retrogression and re-aging heat treatment (RRA) on the A206 alloy and observed better behavior only in the first 48 h of immersion in NaCl, than when compared to the same alloy in an as-cast state. This issue is explained by a higher intensity of attack by intergranular exfoliation of heat-treated Alloy 206 as shown in Figure 9.

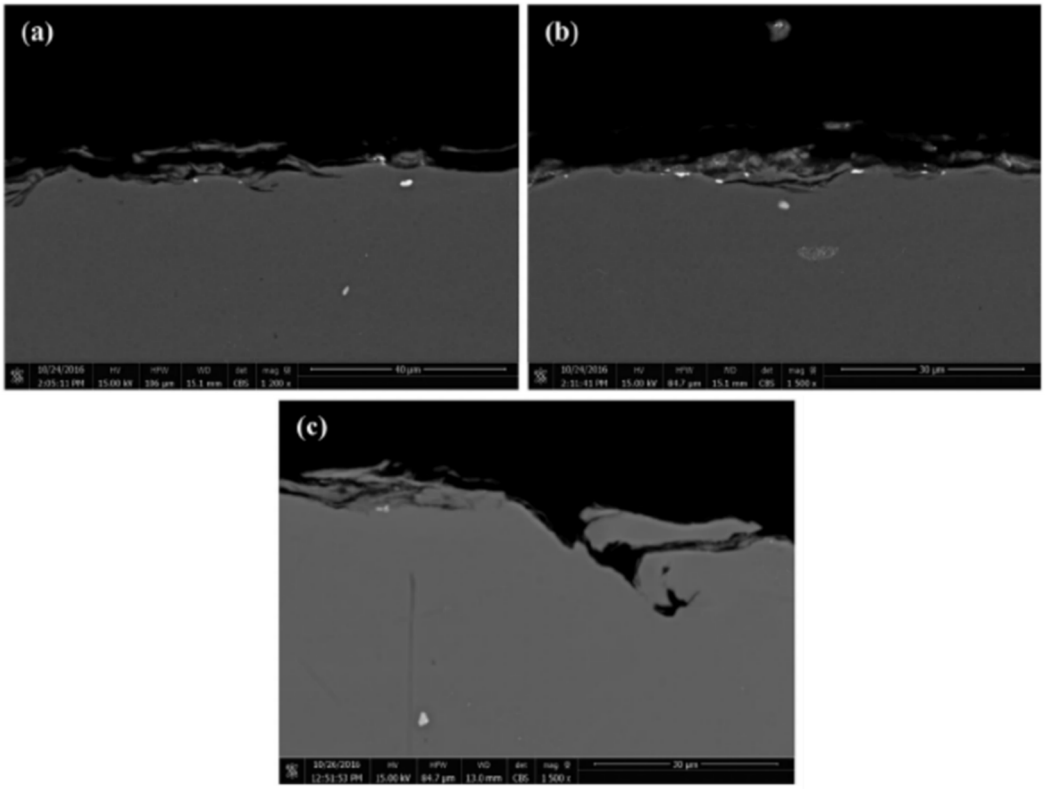

Figure 9. Scanning electron micrographs of the cross section of the RRA B206 aluminum alloy after m 48 h of immersion in artificial seawater showing exfoliation corrosion for a scale bar of 40 μm (**a**) and 30 μm (**b**,**c**). Reprinted with permission of [21].

2.2.3. Series 4xx.x

The aluminum casting alloys of the 400 series are mainly used for their ease of casting and no special mechanical properties are required. Thus, these alloys are only used when the manufacture of complex parts is required. In this regard, Osorio et al. [22] reported the effect of eutectic modification with Na and T4 treatment on the corrosion resistance of a 9% Si-Al alloy.

In the as-cast state, they measured a lower corrosion rate (0.98 μA/cm^2) in the unmodified alloy compared to the modified alloy (3.43 μA/cm^2) which was associated with the formation of a greater interface between the silicon particles and the aluminum phase in the eutectic zone. On the contrary, the effect of the T4 heat treatment caused a spheroidization effect of silicon particles causing a decrease in corrosion rate for the modified alloy from 3.43 μA/cm^2 to 1.75 μA/cm^2.

2.2.4. Series 5xx.x

Al-Mg alloys are characterized by their high resistance to corrosion which makes them suitable for applications in corrosive environments such as the marine sector. Okayasu et al. [23] studied the

corrosion resistance of an A514 alloy (Mg:3%, Si:1%) obtained by heated mold continuous (HMC) and permanent mold. They detected severe intergranular corrosion especially in the precipitates free zone (PFZ) and in the eutectic zone formed by Mg_2Al and Al_6MnFe. In Figure 10 shows how in both cases the A514 alloy has suffered intergranular corrosion in the eutectic zone formed by Mg2Al and Al6MnFe. Moreover, they measured a significantly higher corrosion rate in the gravity castings (80 mg/cm^{2}year) than in the alloy obtained by HMC (40 mg/cm^{2}year) after 336 h in immersion test (5%NaCl, 0.3%H_2O_2), which they associated with the fact that the higher cooling rate led to a higher proportion of solid solution for the HMC castings method. It is important to remark that the resultant cooling rate depends on size and geometry of the specimens, being an average maximum of 132 °C min^{-1}.

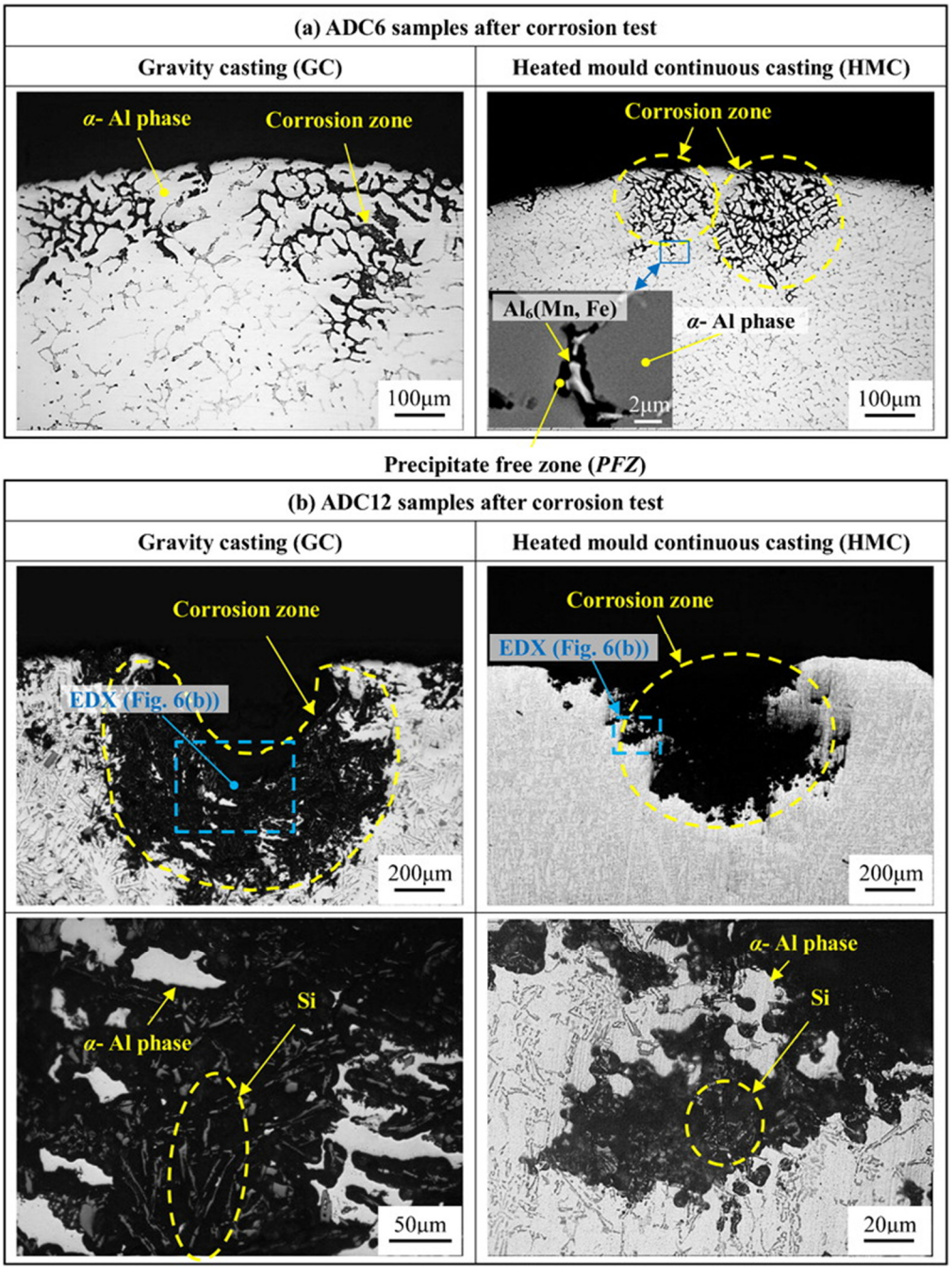

Figure 10. Optical micrographs of cast aluminum alloys after corrosion tests. Reprinted with permission of [23].

2.2.5. Series 9xx.x

The hypoeutectic Ni-Al alloys present a microstructure consisting of a dendritic matrix rich in α-phase aluminum and a eutectic microconstituent composed of α-phase and Al-Ni intermetallics. Al-Ni intermetallic compounds significantly increase the strength of nickel aluminum alloys but, on the other hand, decrease toughness and corrosion resistance. Osorio et al. [24] studied a 5% nickel aluminum alloy produced by directional solidification resulting in a columnar macrostructure as shown in Figure 11.

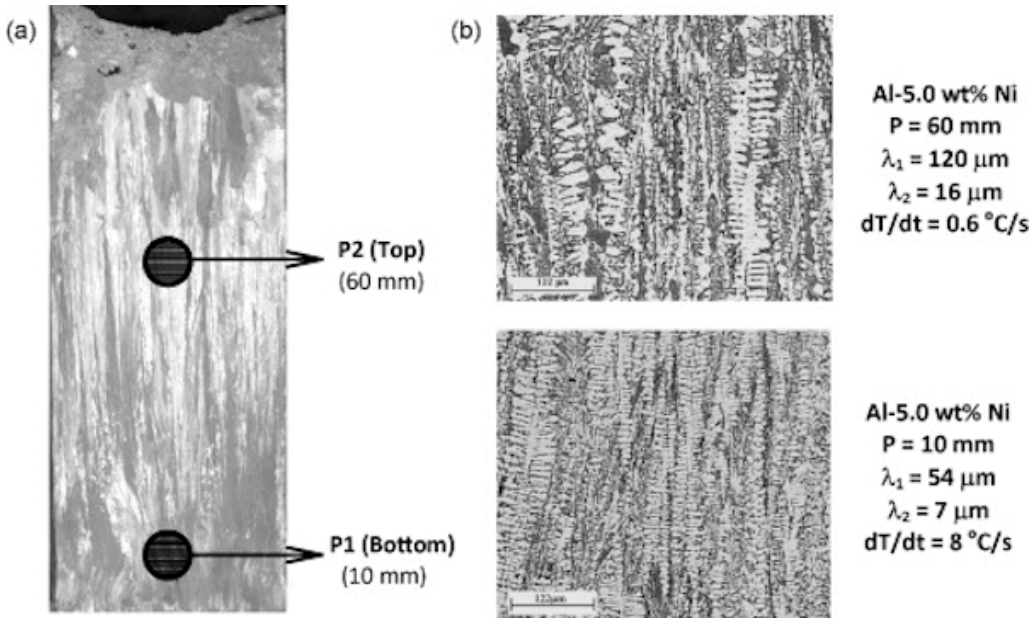

Figure 11. (**a**) Typical macrostructure of the as-cast Al–5 wt % Ni alloy and schematic representation of positions from where the samples were extracted for corrosion tests and (**b**) optical micrographs with corresponding dendritic spacings (λ_1 and λ_2 are the primary and secondary dendritic spacings, respectively) and cooling rates. Reprinted with permission of [24].

Samples were taken in two different positions, one closer to the edge of the mold (P1 = 10 mm), a high cooling rate (8 °C/s) and one further from the edge of the mold (P2 = 60 mm) at a slow cooling rate (0.6 °C/s). The uniform corrosion density obtained in the coarse microstructure (P2) of the nickel aluminum alloy was lower (1.5 μA/cm^2) than the fine microstructure (3.5 μA/cm^2). However, resistance to pitting corrosion was better in the finer microstructure. They associated this finding with the higher eutectic microconstituent fraction and therefore a higher quantity of finer and homogeneously distributed Al-Ni intermetallics.

3. Corrosion Resistance of Cast Aluminum Alloys Obtained by Semi Solid Manufacturing (SSM)

Semisolid metal (SSM) processing is a viable technology in producing a large variety of near net-shape products, in particular for the automotive industry [25] and aerospace [26] sectors. This process is based on using the semisolid behavior of metallic alloys as well as reducing macrosegregation, porosity, and forming forces. Since its discovery in the early 1970s, a wide spectrum of procedures and processes has been developed [27]. The main aim of SSM is to obtain a semisolid structure, characterized by a free dendrite microstructure, with the solid present in a near spherical form. This semisolid mixture flows homogeneously, as a thixotropic fluid with viscosity depending on the shear rate and fraction of solid [28].The nature of the SSM slurry with solid spherical grains suspended in liquid makes it susceptible to liquid segregation during forming processes. There are two methods of SSM known as rheocasting and thixocasting, which are very well identified with their own advantages and disadvantages for particular component purposes [28–30].

SSM processing is in permanent competition with classical cast and machine from forging in manufacturing, in particular automotive complex components. A deep comparative study has been done by Zhu et al. [31] showing the high performance of SSM from financial, technological, and future perspectives issues, with practical application of turbocharger compressor wheels as examples of complex geometric components. There are numerous metallic systems prone to being manufactured by SSM process, such as magnesium alloys [32] and stainless steels [33].

Al is one of the most abundant elements in the earth's crust, but its corrosion resistance restricts the wide usage of aluminum alloys independent of the manufacturing process used. Intermetallic compounds play an essential role in the corrosion resistance of these alloys, related to their size, composition, and the nature of these secondary phase particles, playing an important role in pitting corrosion [34]. Aluminum alloys with silicon as the main alloying element are the most important aluminum alloys utilized in the industrial sector wherein there is a demand for lighter components and this is the reason for looking for improvements in SSM technique process performance in recent years. With this purpose, Salleh et al. [35] has done an overview of semisolid processing of aluminum alloys, pointing out the need to establish studies to modify alloy composition and to characterize processing variables for successful SSM processing rating costs of this technique. Suitable Al-Si modified alloys with precipitation of intermetallic phases that dissolve in the semisolid zone have been proposed as potential material for semisolid processing by Salleh et al. [35].

Al–Si alloys generally suffer localized corrosion in the Al–Si eutectic due to impurities, such as Fe; generally, the corrosion behavior of these alloys depends on the amount and morphology of Fe-rich intermetallics, such as AlFeSi and AlFeSiMg [36]. Both Fe and Si are cathodic with respect to the aluminum, and therefore, together they can form a microgalvanic couple, resulting in localized corrosion, and silicon also increases the corrosion potential [37,38]. The addition of Pb and Cu to Al-Si alloys decreases the corrosion potential and increases current density as has been observed in PM Al-Si alloys. Furthermore, the addition of Pb stabilizes the passive layer [39].

There are few studies reporting on the corrosion behavior of aluminum SSM processed in comparison with alternative processing technologies. Recently, Yang et al. [40] has shown the benefits of applied blast treatment on surface of a SSM319s aluminum alloy. It provokes a decrease of uniform corrosion rate such as strongly inhibiting the occurrence of pit corrosion by salt spray atmosphere tests. It is associated with the surface deformation effects and the existence of residual compressive stress at surface layer [20]. By EDS analysis, the authors observed Al_2O_3 and Al_2O_3 plus $MgCl_2$ as main surface corrosion product and the inner pitting corrosion products, respectively.

Arrabal et al. [41] have reported an effect of Fe rich intermetallic particles on corrosion behavior of rheocast (RC) and gravity-cast (GC) A356 alloy demonstrating that corrosion initiates at the interface between the α-Al matrix and Fe-containing intermetallics as a result of microgalvanic corrosion processes, being pit nucleation critical sites, whereas Si/ α-Al interfaces and primary α-Al dendrites/globules remained unattacked. For longer immersion times, corrosion attack progressed through the eutectic areas. These authors conclude that the A356 rheocast alloy is more resistant to pitting corrosion than the A356 gravity-cast alloy. They attributed this to the reduced potential differences between Si/Fe-rich intermetallic and the eutectic aluminum phase. Figure 12 shows the cyclic polarization curves of these alloys after immersion test in 3.5% NaCl naturally-aerated solution that corroborate this observation.

Mingo et al. [42] has advanced in the Fe rich intermetallic role on rheocasting Al alloys corrosion behavior. In particular by monitoring the size and morphology of these particles, it was observed that the cathodic reaction that takes place over the cathodic particles leads to a local alkalization that destabilizes the adjacent passive layer of the Al matrix, and promotes Al oxidation to Al^{3+} Additionally, the hydrolysis of Al^{3+} produces H^+ that acidifies the bottom area of the trench, inhibiting repassivation, and promoting the corrosion advance. The proximity of intermetallic particles networks, allows the progression of the attack, creating a narrow path of corrosion around it; therefore, intermetallic particles act as a real and dangerous guide for corrosion progression.

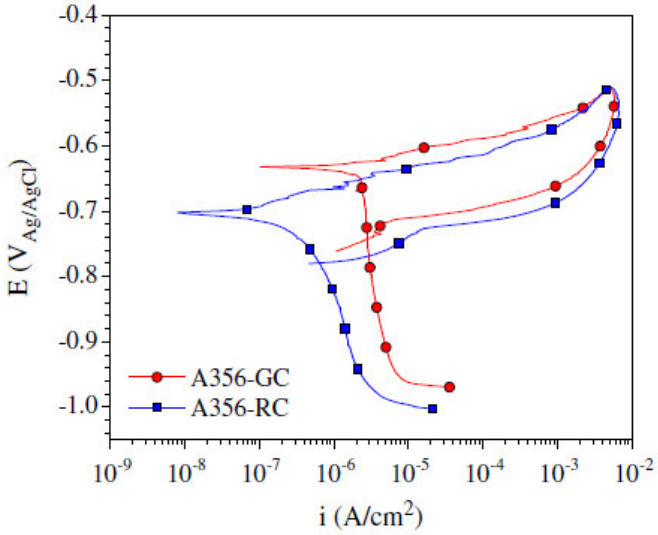

Figure 12. Cyclic polarization curves of A356-GC and A-356-RC aluminum alloys after 1 h immersion in 3.5% NaCl naturally aerated solution. Reprinted with permission of [41].

Eslami et al. [43] has observed that corrosion susceptibility of Al-Si alloys rheocasting SSM processed is influenced by heterogeneous segregation of Al rich phases that controls the electrochemical behavior of the component supported by potentiodynamic polarization curves and electrochemical impedance spectroscopy (EIS) of the thin wall samples in the diluted Harrison solution to simulate acid rain. Corrosion was localized, and a galvanic couple between the eutectic silicon phase and/or Fe-rich intermetallic particles and aluminum matrix was observed (Figure 13).

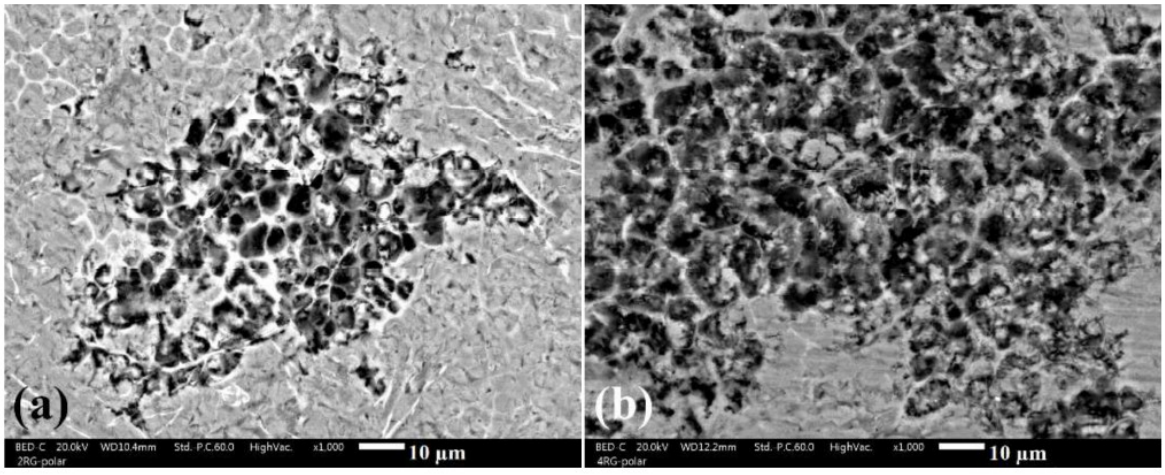

Figure 13. Corroded surfaces of (**a**) 2.5RG and (**b**) 4.5 RG after polarization test in the diluted Harrison solution. Reprinted with permission of [43].

These results are in accordance with the results of other researchers about corrosion of Al–Si alloys in similar solutions [21,25]. They solved this problem by applying surface modification by ground to eliminate an observed purely liquid microstructure´s surface due to the segregation surface which makes them more resistant to corrosion when ground and therefore without surface defects. Nevertheless, selective laser sintering (SLS) layer conducts to heterogeneity of properties in semi-solid metal (SSM) components which are difficult to avoid including after thermal treatments [44].

Tahamtan et al. [45] observed that resistance to pitting corrosion was largely improved due to the reduced area ratio between noble silicon particles and the less-noble eutectic aluminum phase

around silicon particles in a thixoformed A356 alloy in comparison with rheocasting and gravity cast A356 alloy. The results were supported by microstructural observation after electrochemical measurements by linear sweep voltammetry (LSV), establishing a parameter that involves as defects volume (porosity), silicon particle areas, their distances to control pits size and distribution on alloy surface, and their protective character. Table S5 summarizes the relationship between different corrosion test and detection techniques to assess the corrosion behavior of SSM aluminum alloys. Potentiodynamic polarization as EIS using different solutions are the most employed test to check corrosion susceptibility, identified mainly by SEM and EDX techniques.

4. Corrosion Resistance of Cast Aluminum Alloys Obtained by Additive Manufacturing (AM)

Metal additive manufacturing (AM) [46], also known as 3D printing, is a promising technology that has gained interest due to its ability to produce complex components in a fast and suitable way, reducing waste associated with traditional manufacturing methods, associated with plastic deformation or cast. AM often involves the deposition of layers of an alloy feedstock in the form of powders or wires, which are melted together by a rapidly moving heat source to form a solid mass. Successive layers are built up to produce a 3D component [47]. The rate of solidification is often an order of magnitude higher than that seen during conventional casting techniques, and the process of building up layers causes non-uniform cooling, which, in turn, leads to large temperature gradients or thermal stresses in the alloy.

Current methods, such as selective laser sintering (SLS), electron beam melting (EBM), laser powder bed fusion (LPBF), and direct metal laser sintering (DMLS), also known as selective laser melting (SLM) or laser metal fusion (LMF), use a powder-bed based additive manufacturing (AM) technique, which allows fully dense near net-shape parts to be obtained thanks to a powerful laser source able to melt and consolidate the powders layer by layer. Herzog et al. [48] present an overview focusing on the complex relationship between AM processes, microstructures, and the resulting properties for metals, detailing the fundamentals of different methods. Ni et al. [49] dealt with the influence of SLM process parameters regarding Hastelloy alloy, while Mertens et al. [50] review the recent developments of additive manufactured Al components, noting the strong out-of-equilibrium microstructures of these systems.

Nevertheless, all have many intrinsic limitations: the nature of their particular processes; a proper material selection; consideration of elevated cost; defects such as porosity [51], residual stresses, the finishing quality of metal parts, and low deposition rates are some pending issues which are currently barriers to estimating when these methods will be candidates to be used for the fabrication of engineering products. Martin et al. [52] has recently discovered that introducing nanoparticles of nucleants can control solidification during additive manufacturing, avoiding intolerable microstructures with large columnar grains and periodic cracks, associated with the process [52]. Furthermore, the robotics sector has studied the effect of changing the scan speed on the formation of fusion lines and single tracks from an Al alloy to offer an important porosity reduction [53,54]. Recently, Tarnawsky and Yoder claim “no more tears for metal 3D printing” due to these realistic solutions to new problems pending resolution [55].

Corrosion behavior of AM alloys are mainly devoted to Ti and Mg base alloys due to their intrinsic application in automotive, aeronautic, and biomedicine fields [56–61].

Al SLM components are well characterized related to mechanical properties as a result of precise microstructural characterization, [62–64]; in general, higher mechanical response related to cast specimens for different Al base alloys has been observed. So far, very few works have focused on corrosion behavior of additive manufactured Al alloys. Thus, a comprehensive recompilation of the most interesting found features is required. Recently, Suryawanshi et al. [65] have done a comparative study of laser melted ferrous and non-ferrous alloys including Al-Si systems.

Nevertheless, nowadays corrosion behavior of AM components is still pending in depth study. The interaction with the environment is not well documented, which poses potential impact on performance and integrity. The knowledge accumulated thanks to last year´s development of the welding process indicates that corrosion properties of additively manufactured metallic parts result

from the intrinsic heterogeneities and microstructural variations from manufacturing processes [22]. Thus, it can be advanced that all issues that affect microstructural changes and induce defects into material affect corrosion susceptibility. Recently, Sander et al. [66] conducted a state of the art review to know the scenarios of corrosion of AM alloys, noting that features associated with their own process lead to being potential nucleation corrosion sites, such as dislocation networks, grain directionality, solute segregation, porosity, oxides and atypical inclusions, surface roughness, residual stresses, etc. [23]. In addition, Kong et al. [67] do a comparative and critical review of the current state of the knowledge and handicaps pending resolution related to lack of AM corrosion behavior of ferrous and non-ferrous components. They note the main effect of called molten pool boundaries (MPBs), intrinsic to some kind of AM that imply the existence of chemical elemental segregation, thermal stress, and non-equilibrium phases that can exist at the MPBs; both defects comprise of the corrosion behavior of AM components [24]. The authors analyze the performance of additional alternatives for reducing corrosion, such as surface treatments.

Al-base alloys for lightweight applications are perfect candidate materials to be manufactured by AM process, due to their low melting point, density, and high thermal conductivity in comparison with ferrous alloys, but there is significant work to do to advance in this topic, focusing on corrosion associated with AM aluminum alloys. Cast Al-SiMg alloys are widely used in transportation applications—particularly for the automotive, marine, and aerospace industries—because of their high strength and stiffness-to-weight ratio, low density, and good corrosion resistance, and are the most used by AM, in particular by direct metal laser sintering (DMLS) due to fluidity and castability [68,69].

Recently, it has been shown that the microcell technique permits electrochemical measurement in a small spatial scale, and it can be considered a promising non-destructive testing method for additively manufacturing metallic final part, evaluating with high performance susceptibility to localized corrosion susceptibility for different metallic systems [70]. The most commonly studied Al alloy in AM is AlSi10Mg although other systems are by potential application such as Al-Cu and Al-Zn alloys [71]. Gu et al. [72] have proposed the wire + arc additive manufacturing (WAAM) as a promising process to save cost and porosity in Al-Cu alloys manufacturing.

Leon et al. [73] conducted a low cycle fatigue corrosion resistance study of SLM AlSi10Mg alloy, observing that it was relatively poor due to the large amount of cavities and other surface defects generated at the external surface during the process. This leads to a localized corrosion attack in the form of pitting, which creates a large number of crack initiation sites. Fast crack propagation could lead to premature corrosion fatigue failure of components. The authors conclude that it is necessary to pay attention to the surface quality and roughness using SLM technique is the main conclusion of the authors in order to prevent crack nucleation [30].

Kubacki et al. [74] compare the atmospheric corrosion susceptibility of printed Al-10Si-Mg alloy to its cast counterpart over a range of heat treatments, performing tests in a salt-fog chamber using a modified G85-A2 and potentiodynamic test. They observed that the corrosion was dominated by a dissolution of Al that appeared to favor a path of least resistance through coarser or more discontinuous regions of the Si network at the melt pool boundary in cast specimens; in addition, post-printing heat treatments are deleterious to the atmospheric corrosion resistance of AM Al-10Si-Mg alloy.

Prashanth et al. [75] studied the effect of annealing on the tribological and corrosion properties of Al–12Si samples produced by selective laser melting (SLM) via sliding and fretting wear tests and weight loss test in different HNO_3 solutions to compare with corresponding cast material. The acidic corrosion behavior of the as-prepared SLM material as well as of the cast samples is similar and the corrosion rate is accelerated by increasing the heat treatment temperature due to the microstructural changes induced. A continuous network of Si characterizing the as-prepared SLM sample transforms into isolated Si particles in the heat-treated SLM specimens, where the size of the hard Si particles increases, and their density decreases with increasing annealing temperature, and the Al–12Si sliding and fretting wear material´s resistance decreases. The corrosion resistance is reduced as a result of

the loss of the connectivity between the Si particles, which in turn allows easier access of the corroding medium to the Al phase, as is presented in Figure 14.

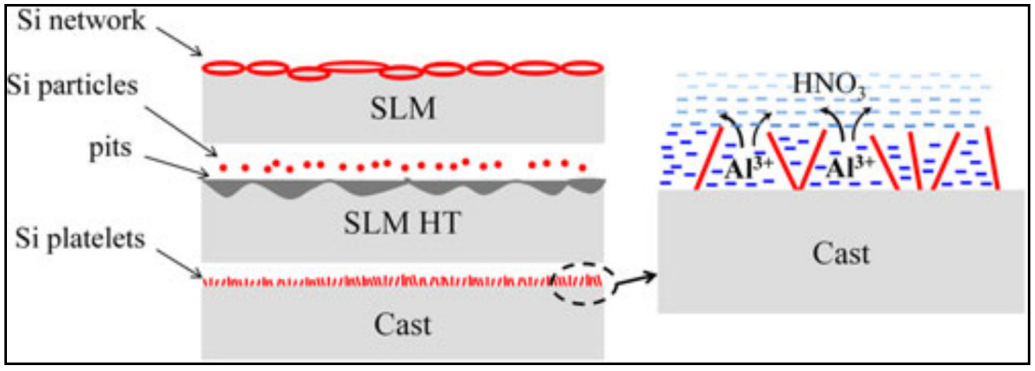

Figure 14. Schematic illustrations showing the corrosion behavior in Al–12Si as-prepared SLM, heat-treated SLM, and the cast samples under acidic environment. Reprinted with permission of [75].

Leon et al. [76] address a comparative study of the corrosion behavior and corrosion fatigue resistance of AlSi10Mg alloy produced by selective laser melting (SLM) and its conventional counterpart, gravity cast alloy, using a 3.5% NaCl solution, checking with immersion test during 45 days and a standard bending machine respectively, observing that the corrosion resistance of the two alloys is relatively similar, with a minor advantage to the printed alloy; meanwhile, AM alloy presents a moderately higher fatigue corrosion related to cast alloy, due to the significant differences between the microstructure and defect characteristics of those two alloys, mainly porosity distribution and the relatively intensive formation of enriched Fe and Mn precipitates with a detrimental microgalvanic effect in cast alloys [33].

Revilla et al. [77] devote attention to an AM by selective laser melting (SLM) novel scandium modified Al-Mg alloy, Al-6.2Mg-0.36Sc-0.09Zr alloy, with a particular emphasis on densification, microstructure and properties, showing that the electrochemical corrosion susceptibility of SLM alloy is lower than cast alloy thanks to the Tafel curves of both specimens, SLM and cast Al-Mg-Sc-Zr tested in aerated 3.5% NaCl solution. The authors observed that the absence of anodic and cathodic active surface reduced the susceptibility to corrosion in the laser molten pool and laser melting modified the grain boundaries to eliminate or minimize Al_3Sc dissolution, hence the overall corrosion resistance has been improved. It is recognized that Sc play an important role on Al alloy properties [78]. Schmidtke et al. [79], propose the new alloy Scalmalloy RP0.66–4.5 with promising aircraft applications.

Girelli et al. [80] address the corrosion behavior of AM AlSi10Mg in chloride bearing environments using electrochemical tests, observing a high dependence with the detected fine network of Si particles uniformly distributed in the Al matrix that ensures a low corrosion current density during the potentiodynamic tests. In contrast, the exposure of machined edges specimens to saline environment leads to a remarkable mass loss, as the consequence of an exfoliation, like corrosion phenomenon, as demonstrated by means of 28-day immersion tests. This problem was solved with T6 thermal treatment.

Cabrini et al. [81] used DMLS to perform specimens of Al-10Si-Mg alloy samples, highlighting a preferential dissolution of α-Al at the border of the laser scan tracks and a slight variation with plane orientation, checked in aerated diluted Harrison solution and using potentiodynamic (PD) tests and electrochemical impedance spectroscopy (EIS) tests. They conclude that the corrosion behavior of DMLS Al–10Si–Mg alloy was due to the roughness, surface porosities and the presence of less protective superficial film formed during process. Ar process atmosphere as isolated particles of aluminum oxide, coming from powder, could inhibit the correct reformation of a continuous film on the surface, interfering with the correct repassivation of aluminum. The negative consequence of this issue is prevented by a shoot peening applied to surface [38]. Cabrini et al. [82] performs

potentiodynamic tests on a AlSi10Mg alloy obtained by LPBF process, observing that an increase of chloride solution concentration provokes a reduction of the pitting potential, with a logarithmic correlation, as indicative of a prone localized corrosion. The authors also detail the positive effect of high temperature post-processing heat treatment to selective dissolution of the α-Al phase stimulated by galvanic coupling with noble silicon precipitates wherein the corrosion morphology of localized attack modifies due to the different distribution and size of silicon phases induced by the heat treatment. Cabrini et al. [83] also reveal the role of silicon precipitates after studying intergranular susceptibility of this alloy based on microstructures, revealing the intergranular corrosion phenomena were less intense for as-produced specimens without heat treatments compared to the heat-treated specimens at 200 °C and 300 °C. Meanwhile, general corrosion morphologies were noted for their higher treatment temperatures [40]. Olakanmi [84] notes the role of aluminum oxide zones on surface could inhibit correct repassivation of aluminum [41].

Fathi et al. [85] show the highest corrosion resistance of a AlSi10MG direct melting laser sintered compared with a die cast A360.1 aluminum based on surface finish influence using potentiodynamic polarization testing and EIS technique in a marine environment. The results highlighted the improved corrosion resistance of the DMLS-AlSi10Mg_200C compared with its cast counterpart with a similar surface finish, known to be dominated by its finer microstructure, and the ground DMLS-AlSi10Mg surface demonstrated the highest resistance to the selective attack, due to the formation of a stable, dense, and thick passive film. The authors propose a post-grinding operation to increase corrosion performance removing porosities. Thus, Rafieazad et al. [86] address the impact of the applied heat-treatment cycles on corrosion resistance of DMLS-AlSi10Mg at an early stage of immersion, in an aerated simulated sea water electrolyte, via anodic polarization testing and electrochemical impedance spectroscopy, revealing more uniformly distributed pitting attack. This finding is attributed to the more protective nature of the passive layer at initial immersion time and severe localized corrosion attacks near the coarse Si particles, due to potential differences between the coalesced Si particles and aluminum matrix galvanic couple after increasing the heat treatment temperature [44].

Fathi et al. [87] shows that in all DMLS-AlSi10Mg samples performed by electrochemical tests in aerated 3.5 wt % NaCl solution, the charge transfer resistance (Rct) was found to be higher than the general passive/corrosion products layer resistance (sum of Rp and Roxide values), confirming that the corrosion behavior is initially more dominated by general uniform corrosion and metastable pitting of the surface than a stable pitting attack. The faster cooling and solidification rate of large MPs in the more stable and compact passive layer sample, limited the coarsening of aluminum dendrites and Si precipitates in the MP regions, leading to a reduction of potential difference between Al and Si phases in that region, provoking less susceptibility of the alloy to both pitting and selective corrosion attacks [45]. In particular, as a non-equilibrium region, selective penetrating has been noted for SLM AlSi10Mg alloy, since isolated silicon particles can gather inside the melt pool borders [88,89].

Gu et al. [90] show a so-called "anisotropic corrosion resistance" of the SLM produced Al-Mg-Sc-Zr alloy related to the quite different microstructures on different planes, which include the molten pool boundary density, $Al_3(Sc,Zr)$ precipitation distribution such as local cathodes that promotes propagation of pits, grain size distribution, and crystallographic orientation after conducted electrochemical tests in 3.5 wt % NaCl solution.

Zhang et al. [91] address an improved corrosion resistance, such as pitting and IGC susceptibility then heat-treating specimen after applying electrochemical tests on Al-Mg-Sc-Zr specimens, observing massive pit areas formed along molten pool boundaries regarding the refined grain size and aggregation of precipitations. In addition, the authors observed other different corrosion morphologies. Zhang et al. [92] correlate the size of island surface with corrosion resistance for the new and promising AlMgScZr alloy based on potenciodynamic tests and pitting corrosion value.

Kordijazi et al. [93] have recently studied a potential application of Al-Cu alloy, A205, as the matrix for a composite material using AM. The electrolyte used for the potentiodynamic polarization corrosion test was 3.5% NaCl solution, and the results show that corrosion resistance increases with

high solidification time values. This is due to an increase of grain size and a consequent decrease in the number of grain boundaries in the alloy matrix; with the section thickness being also influenced. Intergranular corrosion was observed as the main mechanism of degradation [51].

Gharbi et al. [94] obtained by AESEC potentiodynamic polarization. The Al corrosion rate at OCP was about 5 times lower for the AM2024, Al-Cu-Si, as compared to the AA2024-T3, due to second particles precipitation during the process and their role as cathodes. The dissolution of the Cu-rich alloying elements at the early stages of the corrosion is beneficial as it minimizes the growth of potentially large cathodes that would provoke further localized corrosion [52]. AM2024, by laser melting, form a thicker and more stable protective oxide film upon its surface, as it has been previously reported by Revilla et al. [77] using a AlSi10Mg processed via SLM. Iwao et al. [95] observe a decreasing of intergranular corrosion susceptibility of Al-Mn-Si-Cu-Mg alloy, which is caused by smaller potential differences between the neighborhood of grain boundaries and inner grain. In conclusion, additional Mg in Al-Mn-Si-Cu alloy improved not only strength but also corrosion resistance after heat-treatment at higher temperatures such as 473 K. This chemical modification could be taken into account also to avoid intergranular corrosion of AM process components. Table S6 summarizes the relationship between different corrosion test and detection techniques to control corrosion behavior of AM processed aluminum alloys. It can be observed that potentiodynamic polarization in different sodium chloride concentration solutions is the most employed test to check corrosion susceptibility, identified mainly by SEM and EDX techniques.

New methods are reported to reduce porosity level and surface roughness as have been detailed by Ma et al. [96] using the novel technique of ultrasonic nanocrystal surface modification (UNSM) to induce high strain rate plastic deformation on a DMLS-AlSi10Mg metal surface showing a potential benefit for corrosion behavior and wear and fatigue resistance. Atzeni et al. [97] use an abrasive fluidized bed (AFB) finishing of DMLS- AlSi10Mg and Rafieazad et al. [86] to manage a post-printing process as is friction stir processing (FSP) [60].

5. Corrosion Resistance of Coatings Obtained by Different Surface Treatments

Even though Al-Si alloys are difficult to be anodized, the anodizing process is still used as an effective tool to enhance the corrosion and wear resistance for the applications in harsh environments. A representative can be found in [98] where the hardness and corrosion behavior of anodized Al-Si substrate produced by rheocasting is investigated with the aim of understanding the influence of the casting method, segregation, and the anodizing processes parameters on the resultant final properties. It has been demonstrated that the anodizing parameters such as time anodizing and applied voltage directly influence the hardness and corrosion resistance of the oxide layer. In this sense, an increase of the oxide layer is observed by increasing the anodizing time or applied voltage and as a result, a decrease in the hardness and corrosion resistance of the oxide layer is observed. In addition, the corrosion resistance of the oxide layer is strongly influenced by the microstructure of the substrate, as well as on the oxide thickness, in which the eutectic region plays an important role. According to this, the eutectic region acts as a propagation path for the corrosion attack. In Figure 15, it can be clearly appreciated that the corrosion attack is initiated from the surface of the eutectic region and is propagated through the eutectic region where the Si particles may have some defects with surrounded Al_2O_3 matrix.

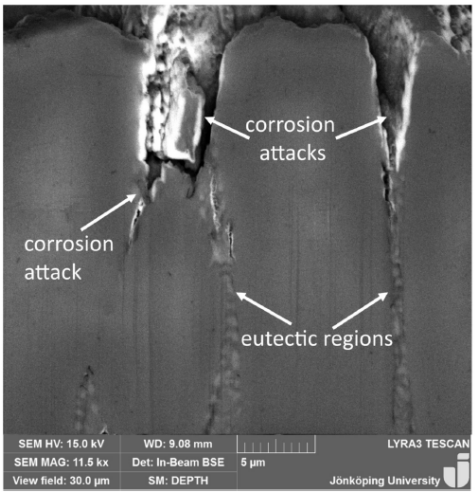

Figure 15. FIB-SEM micrograph of the corroded area in cross-section taken from the anodized sample by liquid casting. Reprinted with permission of [98].

Other interesting work is presented in [99] where the influence of Si content, morphology of Si particles, and cooling rate on anodizing response are evaluated with the aim of investigating the mechanism of formation and growth of the oxide layer on Al-Si casting alloys. In this work, Al-Si based alloys with three levels of Si content were used, the main variables of these materials being the content of Si and level of Sr, which play a key role in the modification of the morphology of Si particles from flake-like to fibrous. In addition, two different cooling rates have also been evaluated to produce samples with two microstructures compared to HPDC and die casting. According to this, secondary dendrite arm spacing (SDAS) is used as a measurement of the local cooling condition because a high cooling rate is referred to the HPDC with an SDAS of around 10 μm, while a low cooling rate is referred to die casting with an SDAS of around 20 μm, respectively. In Figure 16, it can be clearly observed that the aluminum substrates have shown different microstructures as a function of Si content, Si particle morphology, and the resultant cooling rate. Firstly, an increase in the Si content (Figure 16a,b), the Al phase appeared to be refined due to more nucleation of eutectic Si, and the fraction of the eutectic phase increased. Secondly, the addition of Sr has produced a change in the eutectic Si particle morphology from continuous flakes to disconnected smaller fibers (Figure 16b,c). Thirdly, an increase in the cooling rate has contributed to refining both the Al phase and the eutectic phase (Figure 16c,d). In addition, for the fine microstructure (high cooling rate, Figure 16c), the Si particle in the eutectic phase was smaller and more regular in shape compared to the coarse microstructure (low cooling rate, Figure 16d). After performing anodizing, more detailed information about the microstructure of the oxide layers is analyzed by STEM for both unmodified and modified samples of high Si content Al alloys with a high cooling rate, as it can be appreciated in Figures 17 and 18. Once the anodizing process has been performed, several conclusions can be derived. The first one is that the growth of the oxide layer depends on the microstructure of the bulk material and the resultant eutectic phase. In this sense, by limiting the possibility of the oxide layer growing in the eutectic phase, such as decreasing Si concentration and/or decreasing cooling rate, a thicker oxide layer is obtained. The cooling rate could also influence the thickness of the oxide layer by determining the purity of the Al phase. The second one is that during the anodizing process, the Si particle is anodized, but at a lower rate than the Al phase. The oxidation of the Si particle stops when it becomes isolated from the bulk material. The fraction of Si-O depends on the size and morphology of the particle. In the unmodified alloy, the oxide covering the Si particle is displayed as a thin film, while a relatively large fraction of the Si particle is oxidized in the Sr-modified alloy. The Al phase is oxidized faster and the Al_2O_3 grows around the eutectic phase. The different growth rates move the growth direction of the oxide front from the Al phase towards the eutectic phase.

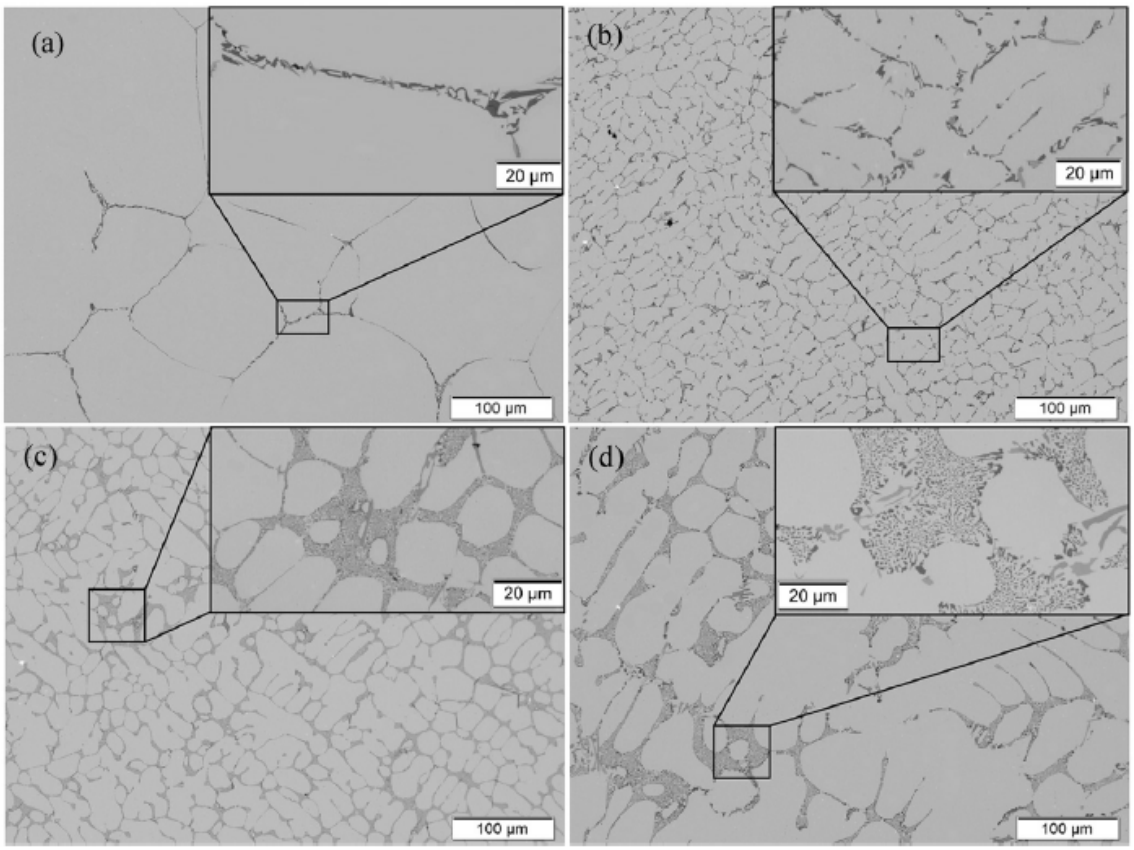

Figure 16. Microstructures of samples: (**a**) alloy A (2.43 wt % Si), high cooling rate; (**b**) alloy C (5.45 wt % Si), high cooling rate; (**c**) alloy C M (5.45 wt % Si), high cooling rate; (**d**) alloy C M (5.45 wt % Si), low cooling rate. Reprinted with permission of [99].

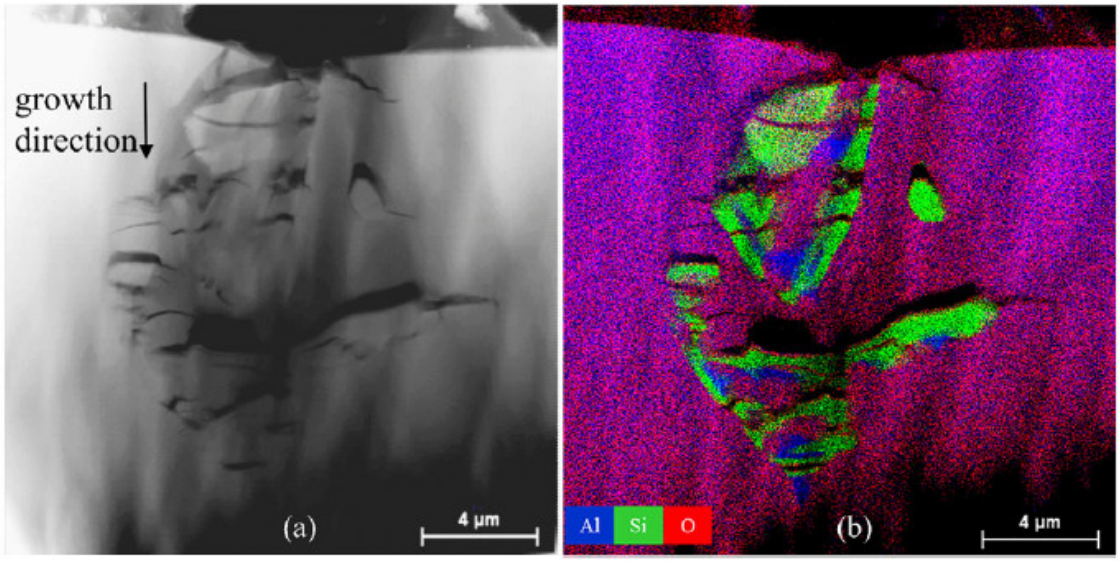

Figure 17. STEM-EDXS micrographs of the anodized layer containing Si flakes (alloy C): (**a**) STEM micrograph; (**b**) EDXS elemental map. Reprinted with permission of [99].

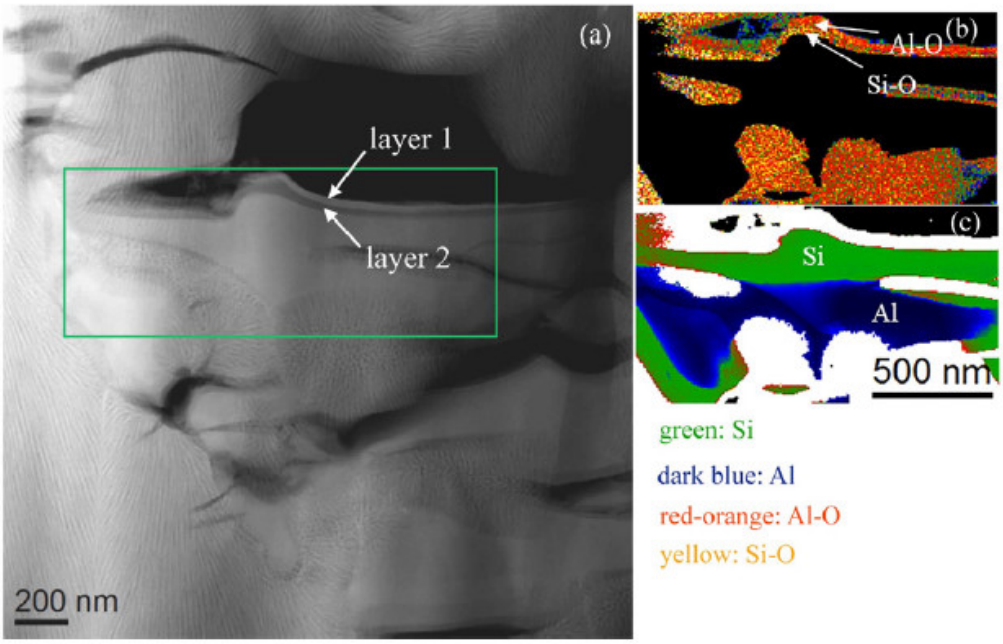

Figure 18. High magnification STEM micrographs of Si flakes inside oxide layer: (**a**) STEM micrograph; (**b**) bulk plasmon energy map of the selected area highlighting the oxide regions; (**c**) bulk plasmon energy map of the selected area highlighting the elemental Si and Al domains. Reprinted with permission of [99].

A promising alternative for surface finishing in terms of long-term stability, wear, and corrosion properties applied onto Al-Si alloys is the plasma electrolytic oxidation (PEO) which is considered as an advanced anodizing process by the application of high voltages and the presence of plasma discharges, respectively [100,101]. The resultant PEO coatings are composed of a three-layered structure for providing the desired properties. The first one consists of a porous outer layer with a low hardness, although it is used for a further post-treatment. The second one consists of an intermediate layer which shows great mechanical and wear resistance. The third one has a barrier layer close to the metallic reference substrate which provides the corrosion resistance [102]. An interesting study is presented in [103] where PEO coatings are developed on A356 (rheocast) aluminum alloy without and with pre-anodizing, being evaluated in terms of characterization, energy consumption, and corrosion behavior. According to this last aspect, PEO coatings developed onto the pre-anodized A356-RC alloy promotes a slower ion exchange at the metal/coating interface, showing a higher inner resistance and lower constant phase element derived from the electrochemical impedance spectroscopy tests. In addition, PEO coatings have improved the corrosion behavior of A356 alloy, and after 4 weeks of immersion, the coating with anodic precursor film has shown the best corrosion resistance. Another interesting study based on PEO of pre-anodized Al-Si alloys is presented in [104] where the corrosion behavior, as well as the effectiveness of different sealing techniques, are evaluated. The use of potassium permanganate and nickel acetate-based sealings have been demonstrated to be the most effective in terms of short and long-term corrosion improvement. In addition, it has also been demonstrated that post-treatments have produced an enhancement in the hydrophobic behavior of the coatings, showing a beneficial effect because the coating impedance has been significantly increased and thereby the susceptibility to corrosion has also been reduced.

Other interesting works are based on an alternative approach of PEO treatment, whereby an aluminum alloy in nitrate molten salt at a temperature of 280 °C is applied [105]. In this work, it has been found that the formed coating was free of any contaminants originating from the electrolytes and had no cracks or pores, which are usually present in coatings formed by PEO treatment in an aqueous solution electrolyte. Other interesting results can be also found in [106] where the coating

obtained in PEO treatment in molten salt consists of hard α-Al_2O_3 and γ-Al_2O_3 phases with a better corrosion resistance three times higher as compared to that treated in aqueous electrolyte solution.

Other interesting surface treatments are based on the use of wet-chemistry technologies such as the sol–gel technology [107]. In [108], hybrid sol–gel silica matrices embedded hallosyte nanotubes with and without cationic corrosion inhibitors (Ce^{3+}/Zr^{4+}) are deposited onto aluminum alloy A356 by using the dip-coating technique. The experimental results have corroborated that the hybrid silica matrix sol–gel coating without any containers has provided good barrier protection only for a shorter duration of exposure to corrosive medium. After performing potentiodynamic polarization curves, it can be observed that after exposure to 120 h, the corrosion current of self-healing (SH) sol coated substrates have been enormously decreased which is the lowest among all, and the corrosion potential has become very much negative. In addition, after prolongated exposure up to 216 h, it has also been observed that the SH sol-coated substrate has exhibited the lowest corrosion current in comparison with the bare reference substrate or even the other coated samples, respectively. These results are in concordance with weight loss measurements where the SH coatings have provided the least corrosion rate, as can be appreciated in Figure 19. Salt fog tests in conjunction with energy dispersive X-ray spectroscopic (EDS) analysis have also been evaluated of the samples of study in order to stablish a comparison of the amounts of C, Si, O, Ce, and Zr on the scribed area before and after the SFT tests. An interesting result is that SH sol-coated substrate has shown more amount of C, Si, Ce, and Zr which clearly reveals that inhibitors have been released into the scratch after the damage, confirming the possible formation of a passive oxide layer and duet to this, the best anticorrosion behavior has been obtained.

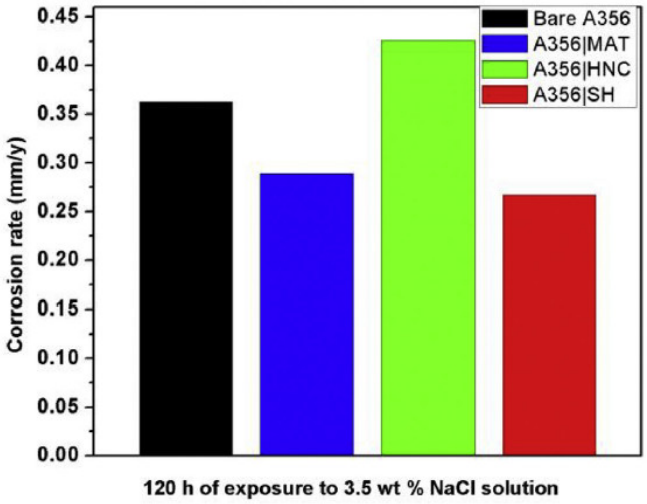

Figure 19. Corrosion rate for coated and uncoated A356.0 substrates after 120 h immersion as determined by weight loss experiments. Reprinted with permission of [108].

Finally, another interesting strategy to obtain prolonged protection is based on the use of a pre-treatment of a metal during its preparation, the chemical conversion coating being a good alternative for this purpose. In [109] zirconium conversion coatings (ZrCC) have been prepared onto aluminum alloy AlSi7Mg0.3 by immersion of the latter in 100–500 ppm baths of hexaflurozirconic acid (H_2ZrF_6). The experimental results have revealed that ZCC formed from 200 ppm H_2ZrF_6 bath (pH = 4.8) with a conversion time of 10 min at room temperature has shown the best corrosion resistance. The resultant ZCC coating presented a bi-layer structure with a thickness of 50–60 nm at the coating matrix and up to 130–150 nm at/around Si crystallites. Finally, it has also been demonstrated that Si from AlSiMg0.3 together with Zr from ZrCC played a key role in self-healing and active corrosion protection, as can be appreciated in the self-healing mechanism derived from ZCC coating in Figure 20. A summary of the different surface treatments can be found in Table S7.

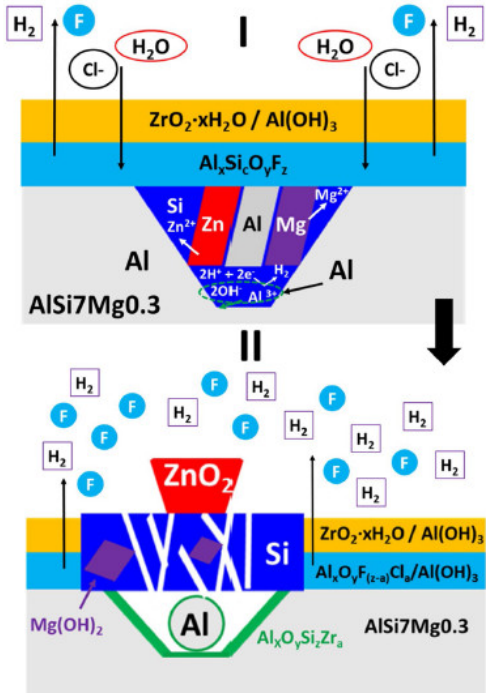

Figure 20. Schematic presentation of the self-sealing mechanism of zirconium conversion coating applied on AlSi7Mg0.3 during its immersion in 0.5 M NaCl solution. Reprinted with permission of [109].

6. Summary and Conclusions

A comprehensive and systematic review has been carried out on the corrosion resistance of cast aluminum alloys. Although in many cases the studies have been quite specific to provide general findings, the following points may be made:

- Corrosion studies of cast aluminum alloys to date have used, in many cases, non-standard alloys in different electrolytes using a range of different corrosion test methods (such as EIS, polarization testing, SKPM, immersion test) making rigorous comparisons difficult. Likewise, there are no studies of long exposures in atmospheric environments, so it is difficult to make long-term predictions.
- In general, corrosion rates measured in neutral chloride media and sulphurated media of cast aluminum alloys can be considered low as they range from 0.5 10–6 to 5. On the contrary, corrosion resistance in basic saline media and acidic media is low.
- The pitting corrosion resistance is not good as the passivation ranges are very small. In addition, intergranular corrosion has also been detected in some studies. This tendency has been observed as the main rule for all aluminum cast series.
- The influence of the characteristic microstructural and macrostructural variables of aluminum alloys—such as grain size, SDAS values, eutectic silicon morphology, and size and nature of intermetallic compounds—on corrosion resistance is complex as there are combined effects between them. In general, higher cooling rates, and the addition of silicon modifier elements improve corrosion resistance while intermetallic compound formation and pore formation decrease corrosion rate. Nevertheless, more work is needed to reach clear conclusions about the individual effect of each microstructural issue on corrosion resistance.
- The addition of rare earth elements (RE) has been shown to improve pitting corrosion resistance as they promote the formation of intermetallic compounds with less tendency to form galvanic couples.

- Corrosion behavior of SSM Al alloys has been checked, demonstrating that mainly Al-Si alloys by rheocasting occupy the major attention in scientific literature, it being that the SSM corrosion performance is higher than cast alloys of identical chemical composition.
- Corrosion study of SSM Al alloys needs more attention since it is a promising technique to obtain close to net final shape of important Al components, mainly of use in the automotive and aerospace industries. Thus, extensive efforts are required to develop tests to characterize corrosion behavior in realistic industrial conditions.
- There is restrictive information about corrosion behavior of AM components in literature. The most studied alloy is AlSi10Mg due to its excellent mechanical strength and corrosion properties in cast state and this has been the basis to be processed by AM. Direct metal laser sintering (DMLS) is the most employed process for this alloy.
- Pitting corrosion is a common form of attack for AM aluminum alloys studied; nevertheless, uniform corrosion, fatigue corrosion and intergranular corrosion have also been observed. Surface roughness associated with AM process must be modified to improve its corrosion behavior. On the other hand, post thermal treatments balance microstructural changes in order to decrease corrosion attack of Al due to the role of cathode Si particles as cathodes.
- Development of new Al alloys with Sc and Zr as promising corrosion resistant materials due to lower level of porosity, controlled microstructure, and good performance against post manufacturing thermal treatment is being observed.
- Different surface treatments—such as anodizing process, sol–gel deposition technique, plasma electrolytic oxidation (PEO), or conversion electrolytic coatings, among others—can be good alternatives for improving the resultant corrosion resistance of the aluminum alloys. The resultant electrochemical corrosion properties have been evaluated in depth for the uncoated and coated materials by using electrochemical techniques such as potentiodynamic curves and electrochemical impedance spectroscopy. In all cases, the coated materials showed remarkably reduced susceptibility to corrosion and significantly increased coating impedance.

Supplementary Materials: The following are available online at www.mdpi.com/2075-4701/10/10/1384/s1.

Author Contributions: Conceptualization, C.B.-L.; methodology, C.B.-L., M.V.B.-M. and P.J.R.; validation, C.B.-L., M.V.B.-M. and P.J.R.; formal analysis, C.B.-L., M.V.B.-M. and P.J.R.; writing—original draft preparation, C.B.-L., M.V.B.-M. and P.J.R.; writing—review and editing, C.B.-L., M.V.B.-M. and P.J.R.; visualization, C.B.-L., M.V.B.-M. and P.J.R.; supervision, C.B.-L., M.V.B.-M. and P.J.R. All authors have read and agreed to the published version of the manuscript.

Funding: This research received no external funding.

Conflicts of Interest: The authors declare no conflict of interest.

References

1. Osório, W.R.; Peixoto, L.C.; Moutinho, D.J.; Gomes, L.G.; Ferreira, I.L.; Garcia, A. Corrosion resistance of directionally solidified Al–6Cu–1Si and Al–8Cu–3Si alloys castings. *Mater. Des.* **2011**, *32*, 3832–3837.
2. Osório, W.R.; Moutinho, D.J.; Peixoto, L.C.; Ferreira, I.L.; Garcia, A. Macrosegregation and microstructure dendritic array affecting the electrochemical behaviour of ternary Al–Cu–Si alloys. *Electrochim. Acta* **2011**, *56*, 8412–8421.
3. Culliton, D.; Betts, A.J.; Kennedy, D. Impact of intermetallic precipitates on the tribological and/or corrosion performance of cast aluminium alloys: A short review. *Int. J. Cast Met. Res.* **2013**, *26*, 65–71.
4. Dobkowska, A.; Cieślak, B.A.; Mizera, J.; Kurzydłowski, K.J.; Kiełbus, A. The Comparison of the Microstructure and Corrosion Resistance of Sand Cast Aluminum Alloys. *Arch. Met. Mater.* **2016**, *61*, 209–212.
5. Öztürk, I.; Ağaoğlu, G.H.; Erzi, E.; Dişpinar, D.; Orhan, G. Effects of strontium addition on the microstructure and corrosion behavior of A356 aluminum alloy. *J. Alloy. Compd.* **2018**, *763*, 384–391.
6. Zor, S.; Zeren, M.; Ozkazanc, H.; Karakulak, E. Effect of Cu content on the corrosion of Al-Si eutectic alloys in acidic solutions. *Anti Corros. Methods Mater.* **2010**, *57*, 185–191.

7. Šekularac, G.; Milošev, I. Corrosion of aluminium alloy AlSi7Mg0.3 in artificial sea water with added sodium sulphide. *Corros. Sci.* **2018**, *144*, 54–73.
8. Panagopoulos, C.; Georgiou, E.P.; Giannakopoulos, K.I. The effect of heat treatment on the corrosion behaviour of 319 aluminium alloy. *Mater. Corros.* **2009**, *60*, 415–418.
9. Arrabal, R.; Mingo, B.; Pardo, A.; Mohedano, M.; Matykina, E.; Merino, M.C.; Rivas, A. Microstructure and corrosion behaviour of A356 aluminium alloy modified with Nd. *Mater. Corros.* **2014**, *66*, 535–541.
10. Liang, Z.; Ye, B.; Zhang, L.; Wang, Q.; Yang, W.; Wang, Q. A new high-strength and corrosion-resistant Al–Si based casting alloy. *Mater. Lett.* **2013**, *97*, 104–107.
11. Zou, Y.; Yan, H.; Yu, B.; Hu, Z. Effect of rare earth Yb on microstructure and corrosion resistance of ADC12 aluminum alloy. *Intermetallocs* **2019**, *110*, 106487, doi:10.1016/j.intermet.2019.106487.
12. Yu, B.-B.; Yan, H.; Zhu, J.-B.; Liu, J.-L.; Li, H.-G.; Nie, Q. Effects of La on Microstructure and Corrosion Behavior of AlSi5Cu1Mg Alloy. *Acta Met. Sin.* **2018**, *32*, 443–451.
13. Colombo, M.; Buzolin, R.H.; Gariboldi, E.; Vallant, R.; Sommitsch, C. Characterization of localized corrosion of heat treated Er- and Zr-containing A356 alloys in 3.5 wt% NaCl aqueous solution. *Mater. Corros.* **2018**, *70*, 246–258.
14. Hu, Z.; Wan, L.; Lü, S.; Zhu, P.; Wu, S. Research on the microstructure, fatigue and corrosion behavior of permanent mold and die cast aluminum alloy. *Mater. Des.* **2014**, *55*, 353–360.
15. Dos Santos, S.L.; Antunes, R.A.; Santos, S.F. Influence of injection temperature and pressure on the microstructure, mechanical and corrosion properties of a AlSiCu alloy processed by HPDC. *Mater. Des.* **2015**, *88*, 1071–1081.
16. Cecchel, S.; Cornacchia, G.; Gelfi, M. Corrosion behavior of primary and secondary AlSi high pressure die casting alloys. *Mater. Corros.* **2017**, *68*, 961–969.
17. Osório, W.R.; Freire, C.M.; Garcia, A. The role of macrostructural morphology and grain size on the corrosion resistance of Zn and Al castings. *Mater. Sci. Eng. A* **2005**, *402*, 22–32.
18. Osório, W.R.; Spinelli, J.E.; Freire, C.M.; Garcia, A. Experimental analysis of corrosion resistance on columnar to equiaxed transition region of as cast structures of Al–Cu alloys. *Mater. Sci. Technol.* **2008**, *24*, 1433–1437.
19. Osório, W.R.; Spinelli, J.E.; Ferreira, I.L.; Garcia, A. The roles of macrosegregation and of dendritic array spacings on the electrochemical behavior of an Al–4.5wt.% Cu alloy. *Electrochim. Acta* **2007**, *52*, 3265–3273.
20. Osório, W.R.; Peixoto, L.C.; Garcia, L.R.; Garcia, A. Corrosion behavior of hypoeutectic Al-Cu alloys in H2SO4 and NaCl solutions. *Acta Met. Sin.* **2009**, *22*, 241–246.
21. Pournazari, S.; Deen, K.; Maijer, D.M.; Asselin, E. Effect of retrogression and re-aging (RRA) heat treatment on the corrosion behavior of B206 aluminum-copper casting alloy. *Mater. Corros.* **2018**, *69*, 998–1015.
22. Osório, W.R.; Garcia, L.R.; Goulart, P.R.; Garcia, A. Effects of eutectic modification and T4 heat treatment on mechanical properties and corrosion resistance of an Al–9wt%Si casting alloy. *Mater. Chem. Phys.* **2007**, *106*, 343–349.
23. Okayasu, M.; Takeuchi, S.; Shiraishi, T. Corrosion and mechanical properties of cast aluminium alloys. *Int. J. Cast Met. Res.* **2013**, *26*, 319–329.
24. Osório, W.R.; Peixoto, L.C.; Cante, M.V.; Garcia, A. Electrochemical corrosion characterization of Al–Ni alloys in a dilute sodium chloride solution. *Electrochim. Acta* **2010**, *55*, 4078–4085.
25. Ivanchev, L.; Wilkins, D.; Govender, G.; Du Preez, W.; Bean, R. Rheo-processing of semi-solid metal alloys: A new technology for manufacturing automotive and aerospace components. *S. Afr. J. Sci.* **2008**, *104*, 257–259.
26. Park, C.; Kim, S.; Kwon, Y.; Lee, Y.; Lee, J. Mechanical and corrosion properties of rheocast and low-pressure cast A356-T6 alloy. *Mater. Sci. Eng. A* **2005**, *391*, 86–94.
27. Atkinson, H.V. Modelling the semisolid processing of metallic alloys. *Prog. Mater. Sci.* **2005**, *50*, 341–412.
28. Flemings, M.; Riek, R.; Young, K. Rheocasting. *Mater. Sci. Eng.* **1976**, *25*, 103–117.
29. Fan, Z. Semisolid metal processing. *Int. Mater. Rev.* **2002**, *47*, 49–85.
30. Qi, M.; Kang, Y.; Zhou, B.; Liao, W.; Zhu, G.-M.; Li, Y.; Li, W. A forced convection stirring process for Rheo-HPDC aluminum and magnesium alloys. *J. Mater. Process. Technol.* **2016**, *234*, 353–367.
31. Zhu, Q.; Midson, S. Semi-solid moulding: Competition to cast and machine from forging in making automotive complex components. *Trans. Nonferrous Met. Soc. China* **2010**, *20*, s1042–s1047.
32. Xing, B.; Li, Y.-D.; Ma, Y.; Hao, Y.; Apelian, D. Commercial AM60 alloy for semisolid processing: Effects of continuous rheoconversion process on microstructure. *Trans. Nonferrous Met. Soc. China* **2010**, *20*, s723–s728.

33. Dao, V.-L.; Zhao, S.-D.; Zhang, Q. Numerical simulation of a thixocasting process for AISI420 stainless steel air-turbine blade. *Trans. Nonferrous Met. Soc. China* **2010**, *20*, s926–s930.
34. Buchheit, R.G.; Grant, R.P.; Hlava, P.F.; McKenzie, B.; Zender, G.L. Local Dissolution Phenomena Associated with S Phase (Al2CuMg) Particles in Aluminum Alloy 2024-T3. *J. Electrochem. Soc.* **2019**, *144*, 2621–2628.
35. Salleh, M.S.; Omar, M.Z.; Syarif, J.; Mohammed, M.N. An Overview of Semisolid Processing of Aluminium Alloys. *ISRN Mater. Sci.* **2013**, *2013*, 1–9.
36. Pech-Canul, M.A.; Giridharagopal, R.; Coral-Escobar, E.E.; Pech-Canul, M.I. Localized Corrosion Behavior of Al-Si-Mg Alloys Used for Fabrication of Aluminum Matrix Composites. *J. Mater. Eng. Perform.* **2013**, *22*, 3922–3932.
37. Reboul, M.C.; Baroux, B. Metallurgical aspects of corrosion resistance of aluminium alloys. *Mater. Corros.* **2010**, *62*, 215–233.
38. Davoodi, A.; Pan, J.; Leygraf, C.; Parvizi, R.; Norgren, S. An insight into the influence of morphological and compositional heterogeneity of an individual intermetallic particle on aluminium alloy corrosion initiation. *Mater. Corros.* **2012**, *64*, 195–198.
39. Lee, C.K. Effects of Pb and Cu additives on microstructure and wear corrosion resistance behaviour of PM Al-Si alloys. *Corros. Eng. Sci. Technol*. **2006**, *41*, 342–352.
40. Yang, F.; He, Y.; Li, D.; Zhu, Q. Salt spray corrosion resistance of SSM319s aluminum alloy with surface blast treatment. *Chin. J. Rare Met.*, **2014,** *38*, 941–947.
41. Arrabal, R.; Mingo, B.; Pardo, A.; Mohedano, M.; Matykina, E.; Rodríguez, I. Pitting corrosion of rheocast A356 aluminium alloy in 3.5wt.% NaCl solution. *Corros. Sci.* **2013**, *73*, 342–355.
42. Mingo, B.; Arrabal, R.; Pardo, A.; Matykina, E.; Skeldon, P. 3D study of intermetallics and their effect on the corrosion morphology of rheocast aluminium alloy. *Mater. Charact.* **2016**, *112*, 122–128.
43. Eslami, M.; Payandeh, M.; Deflorian, F.; Jarfors, A.E.W.; Zanella, C. Effect of Segregation and Surface Condition on Corrosion of Rheo-HPDC Al–Si Alloys. *Metals* **2018**, *8*, 209, doi:10.3390/met8040209.
44. Möller, H.; Curle, U.; Masuku, E. Characterization of surface liquid segregation in SSM-HPDC aluminium alloys 7075, 2024, 6082 and A201. *Trans. Nonferrous Met. Soc. China* **2010**, *20*, s847–s851.
45. Tahamtan, S.; Boostani, A.F. Quantitative analysis of pitting corrosion behavior of thixoformed A356 alloy in chloride medium using electrochemical techniques. *Mater. Des.* **2009**, *30*, 2483–2489.
46. Frazier, W.E. Metal additive manufacturing: A review. *J. Mater. Eng. Perform.* **2004**, *23*, 1917–1928.
47. Rahman Rashid, R.A.; Ali, H.; Palanisamy, S.; Masood, S.H. Effect of process parameters on the surface characteristics of AlSi12 samples made via Selective Laser Melting. *Mater. Today Proc.* **2017**, *4*, 8724–8730.
48. Herzog, D.; Seyda, V.; Wycisk, E.; Emmelmann, C. Additive manufacturing of metals. *Acta Mater.* **2016**, *117*, 371–392.
49. Ni, X.; Kong, D.; Zhang, L.; Dong, C.; Song, J.; Wu, W. Effect of Process Parameters on the Mechanical Properties of Hastelloy X Alloy Fabricated by Selective Laser Melting. *J. Mater. Eng. Perform.* **2019**, *28*, 5533–5540.
50. Mertens, A.; Delahaye, J.; Lecomte-Beckers, J. Fusion-Based Additive Manufacturing for Processing Aluminum Alloys: State-of-the-Art and Challenges. *Adv. Eng. Mater.* **2017**, *19*, 1700003, doi:10.1002/adem.201700003.
51. Galy, C.; Le Guen, E.; Lacoste, E.; Arvieu, C. Main defects observed in aluminum alloy parts produced by SLM: From causes to consequences. *Addit. Manuf.* **2018**, *22*, 165–175.
52. Martin, J.H.; Yahata, B.D.; Hundley, J.M.; Mayer, J.A.; Schaedler, T.A.; Pollock, T.M. 3D printing of high-strength aluminium alloys. *Nat. Cell Biol.* **2017**, *549*, 365–369.
53. Atzeni, E.; Salmi, A. Economics of additive manufacturing for end-usable metal parts. *Int. J. Adv. Manuf. Technol.* **2012**, *62*, 1147–1155.
54. Aboulkhair, N.T.; Maskery, I.; Tuck, C.; Ashcroft, I.; Everitt, N.M. On the formation of AlSi10Mg single tracks and layers in selective laser melting: Microstructure and nano-mechanical properties. *J. Mater. Process. Technol.* **2016**, *230*, 88–98.
55. Tarnawsky, S.P.; Yoder, M.C. No more tears for metal 3D printing. *N. Engl. J. Med*. **2016**, *590*, 726–736.
56. Wegner, N.; Kotzem, D.; Wessarges, Y.; Emminghaus, N.; Hoff, C.; Tenkamp, J.; Hermsdorf, J.; Overmeyer, L.; Walther, F. Corrosion and Corrosion Fatigue Properties of Additively Manufactured Magnesium Alloy WE43 in Comparison to Titanium Alloy Ti-6Al-4V in Physiological Environment. *Materials* **2019**, *12*, 2892, doi:10.3390/ma12182892.

57. Ettefagh, A.H.; Zeng, C.; Guo, S.; Raush, J. Corrosion behavior of additively manufactured Ti-6Al-4V parts and the effect of post annealing. *Addit. Manuf.* **2019**, *28*, 252–258.
58. A, R.; Mitun, D.; Balla, V.K.; Dwaipayan, S.; Devika, D.; Manivasagam, G. Surface properties and cytocompatibility of Ti-6Al-4V fabricated using Laser Engineered Net Shaping. *Mater. Sci. Eng. C* **2019**, *100*, 104–116.
59. Mahamood, R.M.; Akinlabi, E.T. Corrosion behavior of laser additive manufactured titanium alloy. *Int. J. Adv. Manuf. Technol.* **2018**, *99*, 1545–1552.
60. Ivanov, E.; Del Río, E.; Kapchemnko, I.; Nyström, M.; Kotila, J. Development of Bio-Compatible Beta Ti Alloy Powders for Additive Manufacturing for Application in Patient-Specific Orthopedic Implants. *Key Eng. Mater.* **2018**, *770*, 9–17.
61. Han, S.; Zielewski, M.; Holguin, D.M.; Parra, M.M.; Kim, N. Optimization of AZ91D Process and Corrosion Resistance Using Wire Arc Additive Manufacturing. *Appl. Sci.* **2018**, *8*, 1306, doi:10.3390/app8081306.
62. Kaban, I.; Scudino, S.; Eckert, J. Defining the tensile properties of Al-12Si parts produced by selective laser melting. *Acta Mater.* **2017**, *126*, 25–35.
63. Kimura, T.; Nakamoto, T. Microstructures and mechanical properties of A356 (AlSi7Mg0.3) aluminum alloy fabricated by selective laser melting. *Mater. Des.* **2016**, *89*, 1294–1301.
64. Lee, H.-S.; Kumar, A.; Mandal, S.; Singh, J.K.; Aslam, F.; Alyousef, R.; Alabduljabbar, H. Effect of Sodium Phosphate and Calcium Nitrate Sealing Treatment on Microstructure and Corrosion Resistance of Wire Arc Sprayed Aluminum Coatings. *Coatings* **2020**, *10*, 33, doi:10.3390/coatings10010033.
65. Suryawanshi, J.; Baskaran, T.; Prakash, O.; Arya, S.; Ramamurty, U. On the corrosion resistance of some selective laser melted alloys. *Materials* **2018**, *3*, 153–161.
66. Sander, G.; Tan, J.; Balan, P.; Gharbi, O.; Feenstra, D.; Singer, L.; Thomas, S.; Kelly, R.; Scully, J.; Birbilis, N. Corrosion of Additively Manufactured Alloys: A Review. *Corrosion* **2018**, *74*, 1318–1350.
67. Kong, D.; Dong, C.; Ni, X.; Li, X. Corrosion of metallic materials fabricated by selective laser melting. *NPJ Mater. Degrad.* **2019**, *3*, 24, doi:10.1038/s41529-019-0086-1.
68. Lee, C.D. Variability in the tensile properties of squeeze-cast Al–Si–Cu–Mg alloy. *Mater. Sci. Eng. A* **2008**, *488*, 296–302.
69. Li, B.; Wang, H.; Jie, J.; Wei, Z. Effects of yttrium and heat treatment on the microstructure and tensile properties of Al–7.5Si–0.5Mg alloy. *Mater. Des.* **2011**, *32*, 1617–1622, doi:10.1016/j.matdes.2010.08.040.
70. Cao, L.; Panindre, A. Characterization of corrosion behavior on additively manufactured alloys. In *Corrosion*; NACE International: New Orleans, LA, USA, 2017.
71. Bartkowiak, K.; Ullrich, S.; Frick, T.; Schmidt, M. New Developments of Laser Processing Aluminium Alloys via Additive Manufacturing Technique. *Phys. Procedia* **2011**, *12*, 393–401, doi:10.1016/j.phpro.2011.03.050.
72. Gu, J.; Cong, B.; Ding, J.; Williams, S.W.; Zhai, Y. Wire+Arc Additive Manufacturing of Aluminium. In Proceedings of the SFF Symposium Austin Texas, Austin, TX, USA, 6 August 2014; pp. 451–458.
73. Leon, A.; Aghion, E. Effect of surface roughness on corrosion fatigue performance of AlSi10Mg alloy produced by Selective Laser Melting (SLM). *Mater. Charact.* **2017**, *131*, 188–194.
74. Kubacki, G.; Brownhill, J.P.; Kelly, R.G. Comparison of Atmospheric Corrosion of Additively Manufactured and Cast Al-10Si-Mg Over a Range of Heat Treatments. *Corrosion* **2019**, *75*, 1527–1540.
75. Prashanth, K.; Debalina, B.; Wang, Z.; Gostin, P.; Gebert, A.; Calin, M.; Kühn, U.; Kamaraj, M.; Scudino, S.; Eckert, J. Tribological and corrosion properties of Al–12Si produced by selective laser melting. *J. Mater. Res.* **2014**, *29*, 2044–2054.
76. Leon, A.; Shirizly, A.; Aghion, E. Corrosion Behavior of AlSi10Mg Alloy Produced by Additive Manufacturing (AM) vs. Its Counterpart Gravity Cast Alloy. *Metals* **2016**, *6*, 148, doi:10.3390/met6070148.
77. Revilla, R.I.; Liang, J.; Godet, S.; De Graeve, I. Local Corrosion Behavior of Additive Manufactured AlSiMg Alloy Assessed by SEM and SKPFM. *J. Electrochem. Soc.* **2016**, *164*, C27–C35.
78. Zhou, S.; Zhang, Z.; Li, M.; Pan, D.; Su, H.; Du, X.; Li, P.; Wu, Y. Effect of Sc on microstructure and mechanical properties of as-cast Al–Mg alloys. *Mater. Des.* **2016**, *90*, 1077–1084.
79. Schmidtke, K.; Palm, F.; Hawkins, A.; Emmelmann, C. Process and Mechanical Properties: Applicability of a Scandium modified Al-alloy for Laser Additive Manufacturing. *Phys. Procedia* **2011**, *12*, 369–374.
80. Girelli, L.; Tocci, M.; Conte, M.; Giovanardi, R.; Veronesi, P.; Gelfi, M.; Pola, A. Effect of the T6 heat treatment on corrosion behavior of additive manufactured and gravity cast AlSi10Mg alloy. *Mater. Corros.* **2019**, *70*, 1808–1816.

81. Cabrini, M.; Lorenzi, S.; Pastore, T.; Pellegrini, S.; Manfredi, D.G.; Fino, P.; Biamino, S.; Badini, C.F. Evaluation of corrosion resistance of Al–10Si–Mg alloy obtained by means of Direct Metal Laser Sintering. *J. Mater. Process. Technol.* **2016**, *231*, 326–335.
82. Cabrini, M.; Lorenzi, S.; Pastore, T.; Testa, C.; Manfredi, D.; Cattano, G.; Calignano, F. Corrosion resistance in chloride solution of the AlSi10Mg alloy obtained by means of LPBF. *Surf. Interface Anal.* **2018**, *51*, 1159–1164.
83. Cabrini, M.; Calignano, F.; Fino, P.; Lorenzi, S.; Lorusso, M.; Manfredi, D.; Testa, C.; Pastore, T. Corrosion Behavior of Heat-Treated AlSi10Mg Manufactured by Laser Powder Bed Fusion. *Materials* **2018**, *11*, 1051, doi:10.3390/ma11071051.
84. Olakanmi, E. Selective laser sintering/melting (SLS/SLM) of pure Al, Al–Mg, and Al–Si powders: Effect of processing conditions and powder properties. *J. Mater. Process. Technol.* **2013**, *213*, 1387–1405.
85. Fathi, P.; Mohammadi, M.; Duan, X.; Nasiri, A. Effects of Surface Finishing Procedures on Corrosion Behavior of DMLS-AlSi10Mg_200C Alloy versus Die-Cast A360.1 Aluminum. *JOM* **2019**, *71*, 1748–1759.
86. Rafieazad, M.; Mohammadi, M.; Nasiri, A. On microstructure and early stage corrosion performance of heat treated direct metal laser sintered AlSi10Mg. *Addit. Manuf.* **2019**, *28*, 107–119.
87. Fathi, P.; Rafieazad, M.; Duan, X.; Mohammadi, M.; Nasiri, A. On microstructure and corrosion behaviour of AlSi10Mg alloy with low surface roughness fabricated by direct metal laser sintering. *Corros. Sci.* **2019**, *157*, 126–145.
88. Xing, X.; Duan, X.; Jiang, T.; Wang, J.; Jiang, F. Ultrasonic Peening Treatment Used to Improve Stress Corrosion Resistance of AlSi10Mg Components Fabricated Using Selective Laser Melting. *Metals* **2019**, *9*, 103, doi:10.3390/met9010103.
89. Lancea, C.; Chicos, L.; Zaharia, S.; Pop, M.A.; Semenescu, A.; Florea, B.; Chivu, O.R. Accelerated corrosion analysis of alsi10mg alloy manufactured by Selective Laser Melting (SLM). *Rev. Chim.* **2018**, *69*, 975–981.
90. Gu, D.; Zhang, H.; Dai, D.; Ma, C.; Zhang, H.; Li, Y.; Li, S. Anisotropic corrosion behavior of Sc and Zr modified Al-Mg alloy produced by selective laser melting. *Corros. Sci.* **2020**, *170*, 108657, doi:10.1016/j.corsci.2020.108657.
91. Zhang, H.; Gu, D.; Dai, D.; Ma, C.; Li, Y.; Cao, M.; Li, S. Influence of heat treatment on corrosion behavior of rare earth element Sc modified Al-Mg alloy processed by selective laser melting. *Appl. Surf. Sci.* **2020**, *509*, 145330, doi:10.1016/j.apsusc.2020.145330.
92. Zhang, H.; Gu, D.; Dai, D.; Ma, C.; Li, Y.; Peng, R.; Li, S.; Liu, G.; Yang, B. Influence of scanning strategy and parameter on microstructural feature, residual stress and performance of Sc and Zr modified Al–Mg alloy produced by selective laser melting. *Mater. Sci. Eng. A* **2020**, *788*, 139593, doi:10.1016/j.msea.2020.139593.
93. Kordijazi, A.; Weiss, D.; Das, S.; Behera, S.; Roshan, H.M.; Rohatgi, P. Effect of Solidification Time on Microstructure, Wettability, and Corrosion Properties of A205-T7 Aluminum Alloys. *Int. J. Met.* **2020**, 1–11, doi:10.1007/s40962-020-00457-8.
94. Gharbi, O.; Jiang, D.; Feenstra, D.; Kairy, S.; Wu, Y.; Hutchinson, C.; Birbilis, N. On the corrosion of additively manufactured aluminium alloy AA2024 prepared by selective laser melting. *Corros. Sci.* **2018**, *143*, 93–106.
95. Iwao, S.; Asano, M. Effect of Additional Cu and Mg in Al-Mn-Si Alloy on Intergranular Corrosion Susceptibility after Heat-treatment at 200 °C. *J. Jpn. Inst. Light Met.* **2009**, *59*, 108–113.
96. Ma, C.; Dong, Y.; Ye, C. Improving Surface Finish of 3D-printed Metals by Ultrasonic Nanocrystal Surface Modification. *Procedia CIRP* **2016**, *45*, 319–322.
97. Atzeni, E.; Barletta, M.; Calignano, F.; Iuliano, L.; Rubino, G.; Tagliaferri, V. Abrasive Fluidized Bed (AFB) finishing of AlSi10Mg substrates manufactured by Direct Metal Laser Sintering (DMLS). *Addit. Manuf.* **2016**, *10*, 15–23.
98. Zhu, B.; Zanella, C. Hardness and corrosion behaviour of anodised Al-Si produced by rheocasting. *Mater. Des.* **2019**, *173*, 107764, doi:10.1016/j.matdes.2019.107764.
99. Zhu, B.; Seifeddine, S.; Persson, P.O.; Jarfors, A.E.W.; Leisner, P.; Zanella, C. A study of formation and growth of the anodised surface layer on cast Al-Si alloys based on different analytical techniques. *Materials Des.* **2016**, *101*, 254–262.
100. Yerokhin, A.; Nie, X.; Leyland, A.; Matthews, A.; Dowey, S. Plasma electrolysis for surface engineering. *Surf. Coat. Technol.* **1999**, *122*, 73–93.

101. Matykina, E.; Arrabal, R.; Mohedano, M.; Mingo, B.; Gonzalez, J.; Pardo, A.; Merino, M.C. Recent advances in energy efficient PEO processing of aluminium alloys. *Trans. Nonferrous Met. Soc. China* **2017**, *27*, 1439–1454.
102. Arrabal, R.; Mohedano, M.; Matykina, E.; Pardo, A.; Mingo, B.; Merino, M.C. Characterization and wear behaviour of PEO coatings on 6082-T6 aluminium alloy with incorporated α-Al_2O_3 particles. *Surf. Coat. Technol.* **2015**, *269*, 64–73.
103. Mohedano, M.; Matykina, E.; Arrabal, R.; Mingo, B.; Zheludkevich, M.L. PEO of rheocast A356 Al alloy: Energy efficiency and corrosion properties. *Surf. Interface Anal.* **2015**, *48*, 953–959.
104. Mohedano, M.; Matykina, E.; Arrabal, R.; Mingo, B.; Pardo, A. PEO of pre-anodized Al–Si alloys: Corrosion properties and influence of sealings. *Appl. Surf. Sci.* **2015**, *346*, 57–67.
105. Sobolev, A.; Kossenko, A.; Zinigrad, M.; Borodianskiy, K. An Investigation of Oxide Coating Synthesized on an Aluminum Alloy by Plasma Electrolytic Oxidation in Molten Salt. *Appl. Sci.* **2017**, *7*, 889, doi:10.3390/app7090889.
106. Sobolev, A.; Kossenko, A.; Zinigrad, M.; Borodianskiy, K. Comparison of plasma electrolytic oxidation coatings on Al alloy created in aqueous solution and molten salt electrolytes. *Surf. Coat. Technol.* **2018**, *344*, 590–595.
107. Wang, D.; Bierwagen, G.P. Sol–gel coatings on metals for corrosion protection. *Prog. Org. Coat.* **2009**, *64*, 327–338.
108. Manasa, S.; Jyothirmayi, A.; Siva, T.; Sathiyanarayanan, S.; Gobi, K.; Subasri, R. Effect of inhibitor loading into nanocontainer additives of self-healing corrosion protection coatings on aluminum alloy A356.0. *J. Alloy. Compd.* **2017**, *726*, 969–977.
109. Šekularac, G.; Kovač, J.; Milošev, I. Prolonged protection, by zirconium conversion coatings, of AlSi7Mg0.3 aluminium alloy in chloride solution. *Corros. Sci.* **2020**, *169*, 108615, doi:10.1016/j.corsci.2020.108615.